NATIONAL ADVISORY COMMITTEE FOR AERONAUTICS

TECHNICAL NOTE 2359

FLOATING CHARACTERISTICS OF A PLAIN AND A HORN-BALANCED RUDDER AT SPINNING ATTITUDES AS DETERMINED FROM ROTARY TESTS ON A MODEL OF A TYPICAL LOW-WING PERSONAL-OWNER AIRPLANE

By William Bihrle, Jr.

Langley Aeronautical Laboratory
Langley Field, Va.

Washington
May 1951

NATIONAL ADVISORY COMMITTEE FOR AERONAUTICS

TECHNICAL NOTE 2359

FLOATING CHARACTERISTICS OF A PLAIN AND A HORN-BALANCED RUDDER AT SPINNING ATTITUDES AS DETERMINED FROM ROTARY TESTS ON A MODEL OF A TYPICAL LOW-WING PERSONAL-OWNER AIRPLANE

By William Bihrle, Jr.

SUMMARY

An investigation was conducted to determine the floating characteristics of full-length plain and horn-balanced rudders during rotary tests at spinning attitudes on a $\frac{1}{6}$-scale model of a typical low-wing personal-owner airplane. The investigation also included the determination of the effects of the horizontal tail and the wing on the rudder floating characteristics.

The results indicated that the rudder was in the wake of the stalled wing and oscillated violently for the spinning angle-of-attack range from 35° to 55° and that at lower spinning angles of attack the horn-balanced rudder had more desirable floating characteristics than the plain rudder. Neither the plain nor the horn-balanced rudder would fulfill the rudder-deflection requirement for satisfactory spin recovery with controls released as determined from available free-spinning model data. The results also indicated that, if the tail was not in the wake of the wing, the horn-balanced rudder had more favorable floating characteristics than the plain rudder through a large spinning angle-of-attack range for a normal sideslip-angle range. It was shown that horizontal-tail interference led to an appreciable difference between floating angles obtained from static data and from rotary data.

INTRODUCTION

A study of available rudder hinge-moment-coefficient data was made in reference 1 to determine the floating characteristics of various types of rudders in spinning attitudes. The study was made because Civil Air Regulations (reference 2) in force at the time the

study was initiated required spin recovery of personal-owner airplanes with controls released. In order to comply with these regulations, the floating characteristics of a rudder, for any given tail design, would have to be such that the control surface would float against the spin to a position required for satisfactory recovery. Results of free-spinning tests on personal-owner airplane designs (reference 3) indicated that, in general, the rudder must float to large deflections against the spin to ensure satisfactory recovery.

Reference 1, which consisted of limited static hinge-moment data available at spinning attitudes, indicated that the plain rudder had undesirable floating characteristics as regards spin recovery and that use of a horn-balanced rudder appeared promising. Inasmuch as the available data were limited and the reliability of static data in predicting rudder floating characteristics during a spin was not known, the present investigation was made to determine floating characteristics from extensive rotary tests at spinning attitudes. For this investigation, rudder floating angles were measured during rotation of a typical low-wing personal-owner airplane model at spinning attitudes with full-length (part of the rudder extends below the horizontal tail) plain and horn-balanced rudders. Tests were also conducted to determine the interference effects of the horizontal tail and the wing on floating characteristics and these tests were supplemented by some tuft studies. A comparison of the floating angles obtained from rotary tests and those predicted by static tests is also included.

SYMBOLS

The angles, velocities, and spin radius measured on an airplane in a right spin are shown in figure 1.

V	full-scale true rate of descent, feet per second
Ω	full-scale angular velocity about spin axis, revolutions per second
β	sideslip angle at a point on spinning airplane (positive when relative wind comes from right of plane of symmetry), degrees $\left(\sin^{-1}\frac{V_Y}{V_R}\right)$
V_R	resultant local velocity at a point on spinning airplane, feet per second

V_Y	component of resultant local velocity perpendicular to plane of symmetry at a point on spinning airplane, feet per second
ϕ	angle between span axis and horizontal, positive when right wing is down, degrees
α	angle between thrust line and vertical (approx. equal to absolute value of angle of attack at plane of symmetry), degrees
R_s	spin radius, distance from spin axis to center of gravity of airplane, feet
ρ	air density, slugs per cubic foot
q	free-stream dynamic pressure, pounds per square foot $\left(\frac{1}{2}\rho V^2\right)$
S	area of rudder (rearward of hinge line), square feet
S_{horn}	area of horn, square feet
b	rudder height along hinge axis, feet
c	mean geometric chord of rudder (rearward of hinge line), feet
c_{horn}	mean geometric chord of horn, feet
$\bar{c}$	root-mean-square chord of rudder (rearward of hinge line), feet
B	balance coefficient $\left(\sqrt{\frac{S_{horn}c_{horn}}{Sc}}\right)$
C_h	rudder hinge-moment coefficient $(H/qb\bar{c}^2)$
H	rudder hinge moment (positive when it tends to deflect rudder to left)
δ_r	rudder deflection with respect to fin (positive when trailing edge is deflected left), degrees

$(\delta_r)_{C_h=0}$ floating angle, degrees

Subscripts:

cg center of gravity

t tail

MODEL AND APPARATUS

Model

The full-scale dimensional characteristics and a three-view drawing of the typical low-wing personal-owner airplane simulated by the model, which was $\frac{1}{6}$-scale, are given in table I and figure 2, respectively.

A plain and a horn-balanced rudder were investigated on the model. The balanced rudder had a 20-percent-area horn and a balance coefficient B (reference 4) of 0.390. The vertical-tail plan forms were the same for both rudders and had NACA 0009 airfoil sections. The area behind the hinge line was equal for the two rudders; for the balanced rudder, a horn replaced a part of the upper fin area. The bottom edge of the horn was rounded. Dimensions of the full-scale vertical tail with the plain and with the horn-balanced rudders are shown in figure 3. The fins were constructed of solid pine and the rudders were of built-up construction of pine covered with doped paper. Both rudders were mass-balanced.

Apparatus

For the tests the model was set at spinning attitudes on the rotary balance which is installed in the Langley 20-foot free-spinning tunnel and is described in reference 5. A photograph of the model mounted on the rotary balance is shown as figure 4. The rudder was released to float freely from full with the spin (full right rudder in a right spin) during each test by means of a mechanism that was installed in the model. The friction of the rudder hinge system was small and its influence on resulting floating angles was considered negligible. A control-position indicator, located in the rear of the fuselage, transmitted the rudder floating position to a recording oscillograph. A slip-ring and brush arrangement incorporated in the rotary balance was utilized in the operation of the rudder release mechanism and for the transmittal of the rudder floating position.

Nylon tufts were used for the flow studies, and the flow patterns were recorded by a stationary 16-millimeter motion-picture camera equipped with a telephoto lens.

TESTS AND METHODS

The rudder-floating-angle data of this investigation were obtained over an angle-of-attack range from 15° to 65° in 10° increments. For each angle of attack, tests were conducted for combinations of R_s, ϕ, Ω, and V which were chosen after a study of the free-spinning results presented in reference 3 for a model typical of a personal-owner airplane and similar to the model of this investigation. Table II presents full-scale values of R_s, ϕ, Ω, V, and the resulting sideslip at the center of gravity β_{cg} and at the tail β_t for which tests were performed at each angle of attack for both the plain and the horn-balanced rudder for each of the following model configurations:

(a) Vertical tail in the presence of a fuselage, horizontal tail, and wing (complete model)

(b) Vertical tail in the presence of a fuselage (wing and horizontal tail removed)

(c) Vertical tail in the presence of a fuselage and horizontal tail (only wing removed)

The ailerons were set at neutral and the elevators were deflected 30° up for the entire investigation. The maximum rudder deflection range was 30° right to 30° left. Tests were made at an approximate Reynolds number range of 125,000 to 206,000 based on the mean geometric chord of the vertical tail and on the local velocity at the tail.

Tuft studies were made for all model configurations on the outboard and inboard sides of the vertical tail for the horn-balanced rudder at angles of attack of 35° and 45°.

The plain and the horn-balanced rudders were statically mass-balanced, since calculations and preliminary tests showed that, with a statically mass-balanced rudder, centrifugal-force effects on floating angles in a spin were negligible.

The values of β_t were calculated at a point on the tail by the equation $\sin \beta_t = \frac{V_Y}{V_R}$ where V_R (the resultant local velocity at any

point) and V_Y (the component of resultant local velocity perpendicular to plane of symmetry at any point) are functions of the distance between the spin axis and a given point on the spinning model. Inasmuch as this distance varies for different points on the airplane, a variation in sideslip angle is obtained over the vertical tail; therefore in order to refer the floating-angle data to a sideslip angle at the tail, the sideslip at an arbitrary point was chosen. This point on the tail was located at the midpoint of the rudder hinge line.

PRESENTATION OF RESULTS

The floating characteristics of the plain rudder and of the horn-balanced rudder on the complete model are indicated in figure 5. The floating characteristics with the wing and the horizontal tail removed and with only the wing removed are indicated in figures 6 and 7, respectively. In these figures the floating angles of the plain and the horn-balanced rudders are presented as a function of sideslip at the tail for specific angles of attack. When the floating angles were not steady, the midpoint deflection of the oscillations was plotted and the range through which the rudder oscillated was indicated.

Film strips of the tests with tufts on the vertical tail with the horn-balanced rudder are presented in figures 8 and 9 for an angle of attack of 35° and in figures 10 and 11 for an angle of attack of 45°. Studies of the tufts on the outboard side of the vertical tail (left side in a right spin) are shown in figures 8 and 10 and on the inboard side in figures 9 and 11.

Results for the plain rudder when the wing and horizontal tail were removed (fig. 6) are compared with static hinge-moment data determined from reference 6 for a plain rudder (wing, horizontal tail, and fuselage not present) in figure 12. A comparison between the results for the plain rudder when only the wing was removed and data from reference 6 for a plain rudder in the presence of a low and a high horizontal tail (wing and fuselage not present) is presented in figure 13.

RESULTS AND DISCUSSION

Floating Characteristics of the Plain and of the Horn-Balanced Rudders

The results in figures 5 to 7 show that for corresponding tests (same angle of attack, model configuration, and rudder) for equal values of sideslip angle at the tail the floating angles in general were approximately the same even though the amount of sideslip variation over the vertical tail was different because of the different combinations of Ω and V tested. For the practicable combinations of Ω and V used in this investigation, therefore, the amount of sideslip-angle variation over the vertical tail was found to have no appreciable effect on the floating angles, and curves in general could be faired through the test points regardless of the combination of Ω and V employed during each test in obtaining sideslip-angle values at the tail.

Complete model.- The rudder floating data obtained for the complete model (fig. 5) indicated that, for angles of attack of 15° and 25° when either the plain or the horn-balanced rudder was released from full with the spin, the rudder floated to some specific angle. The plain rudder floated with the spin for all values of outward sideslip at the tail, the floating angle becoming progressively more with the spin as the outward sideslip increased. The horn-balanced rudder floated against the spin or floated less with the spin than the plain rudder did. When, however, either rudder was released during spins at angles of attack ranging from 35° to 55°, it did not float to a specific angle but instead oscillated violently through a wide range of rudder angle. Although the relative evaluation of the two rudders was not possible for this angle-of-attack range, it would appear that the horn-balanced rudder did not have more desirable floating characteristics than the plain rudder. At an angle of attack of 65°, the plain and the horn-balanced rudders did not oscillate and floated at approximately the same deflections. In general, therefore, it was indicated that the horn-balanced rudder had more favorable floating characteristics than did the plain rudder for only very low spinning angles of attack.

A study of the tuft pictures for the complete model in figures 8 to 11 showed the presence of turbulent flow in the region of the vertical tail which probably caused the oscillatory motions of the rudders.

In an attempt to determine the cause of the turbulent flow in the region of the vertical tail for the angle-of-attack range from 35° to 55° and to account for the apparent ineffectiveness of the horn above an angle of attack of 25°, the floating characteristics of the rudders were determined with the wing and horizontal tail removed and with only the wing removed.

Wing and horizontal tail removed.- The floating angles measured for the plain and the horn-balanced rudders when the wing and horizontal tail were removed (fig. 6) were steady throughout the spinning angle-of-attack range from 15° to 65°. The plain rudder, for any specific angle of attack, floated with the spin for all values of outward sideslip at the tail; as the outward sideslip at the tail increased, the rudder floated progressively more with the spin and approached a deflection full with the spin. As the angle of attack increased, a deflection full with the spin was attained for lower values of outward sideslip. The horn-balanced rudder, at an angle of attack of 15°, floated against the spin for outward sideslip values up to 20°. As the angle of attack was increased up to 35°, the range of outward sideslip for which the rudder floated against the spin progressively decreased, and for the outward sideslip angles for which the horn-balanced rudder floated with the spin, it floated less with the spin than the plain rudder did. At and above an angle of attack of 45°, however, the horn-balanced rudder floated at approximately the same deflections that were obtained for the plain rudder. It is therefore indicated that, for spins at low angles of attack, the horn-balanced rudder had more favorable floating characteristics than the plain rudder, but the effectiveness of the horn decreased with increasing angle of attack, the horn becoming completely ineffective above an angle of attack of 35°.

The tuft pictures presented herein for angles of attack of 35° and 45° for the wing and the horizontal tail removed showed that the direction of the flow in general was spanwise over the vertical tail; the same result was obtained in reference 6. The tuft pictures obtained on the outboard side of the vertical tail (fig. 8) indicated that the air flow was generally steady for an angle of attack of 35°. The direction of the flow was generally chordwise, however, for outward sideslip values up to approximately 10° apparently because of the presence of the fuselage. As the outward sideslip increased above 10°, the direction of the flow became more spanwise over the tail and assumed approximately the direction of the free-stream flow. On the inboard side of the vertical tail (fig. 9), the air flow was steady at low values of outward sideslip and the direction of the flow was generally chordwise for outward sideslip values up to approximately 10°. For larger outward sideslip angles, the direction of the flow became spanwise, which is similar to the direction of the flow obtained over the upper surface of a sweptback wing. At very large angles of

sideslip, the vertical tail generally became stalled. At an angle of attack of 45° (figs. 10 and 11), it was indicated that, in general, the flow on both outboard and inboard sides was similar to that obtained at an angle of attack of 35°. At the higher angle of attack, however, the flow became more spanwise; this result was more clearly illustrated in reference 6. It is therefore indicated that the effectiveness of the horn in making the rudder float against the spin (fig. 6) was decreased as the flow became spanwise.

Effect of horizontal-tail and wing interference.- The floating angles obtained with the plain and the horn-balanced rudders when the wing was removed (fig. 7) were steady throughout the angle-of-attack range from 15° to 65°. The presence of horizontal-tail interference on the floating characteristics of the rudder is clearly indicated by comparing figure 6 (wing and horizontal tail removed) with figure 7 (wing removed).

For the plain rudder throughout the angle-of-attack range from 15° to 65° for outward sideslips up to approximately 25°, the effect of the horizontal tail was generally such that the rudder floated at deflections which were less with the spin than were obtained with the horizontal tail removed. The difference in floating tendency when the horizontal tail was on and when it was off generally increased as the angle of attack was increased; this increase indicated that the horizontal-tail interference became greater. For angles of attack of 45° and 55° when the outward sideslip was 10° or less, however, a reverse interference effect of the horizontal tail was indicated. No immediate explanation could be found for this condition.

As was the case for the plain rudder, the influence of the horizontal tail was such as to make the horn-balanced rudder float at deflections less with (or farther against) the spin than were obtained with the horizontal tail removed. Also, for the horn-balanced rudder at angles of attack of 45° and 55°, a reverse horizontal-tail interference effect was indicated for outward sideslips less than 10°. The data indicate that the effect of horizontal-tail interference was such that the horn-balanced rudder had more favorable floating characteristics than the plain rudder through a larger angle-of-attack range (up to 55°) for a normal sideslip-angle range. This result might be explained by the fact that the horizontal tail decreased the effectiveness of the rudder area behind the hinge line and thus increased the relative effectiveness of the horn.

A comparison of the tufts for the configurations with the horizontal tail on and off at an angle of attack of 35° (fig. 8) indicates that for outward values of sideslip the horizontal tail modified the flow over the outboard side of the vertical tail just above the horizontal tail.

On the inboard side of the fin (fig. 9), it is indicated that, for the condition with the horizontal tail on, the rudder becomes stalled at lower values of outward sideslip than were obtained for the horizontal-tail-off condition; the rudder became stalled at lower values of outward sideslip because, as was indicated previously, for the horizontal-tail-on condition the rudder floated farther against the spin and the rudder therefore was effectively at a higher control-surface angle of attack. At an angle of attack of 45° (figs. 10 and 11), the flow was similar to that obtained at an angle of attack of 35° except that a greater vertical-tail area on the outboard side was affected by the horizontal tail. This horizontal-tail interference was borne out by pressure-distribution measurements performed on a rotating model of a complete airplane at an angle of attack of 60° which are presented in reference 7; for the angle of attack and tail configuration investigated in reference 7, the vertical tail surfaces were completely in the region of the separated flow from the horizontal-tail upper (suction) surface. It was also shown that the negative pressures on the upper surface of the horizontal tail were higher on the outboard than on the inboard horizontal tail; this difference was caused by the lower angles of attack over the outboard horizontal tail in a spin. Since the vertical tail surfaces were in this pressure region, the negative pressures were greater on the outboard than on the inboard side of the vertical tail. Therefore, the rudder floated more against the spin since the effect of the horizontal tail was such that a larger negative pressure was present on the shielded outboard side than on the shielded inboard side of the rudder.

In this investigation, the assumption was made that the rudder, for a given tail design, that floats farthest against the spin (left in a right spin) is the rudder that has the most desirable floating characteristics for spin recovery with controls released. This assumption was made on the basis that the anti-spin yawing moment contributed by the rudder will be increased as the rudder moves farther against the spin. It should be mentioned, however, that if a rudder floats farther against the spin for one tail design than for another because of horizontal-tail interference, it may not necessarily indicate that the tail design for which the rudder floated farthest against the spin is the more beneficial for spin recovery with controls released. For instance, the total yawing moment contributed by a partial-length rudder (rudder does not extend below the horizontal tail) might be a pro-spin yawing moment if the entire rudder area were in the pressure region of the horizontal tail, since the same pressure differential which causes the rudder to float to a position against the spin also results in a pro-spin yawing moment about the center of gravity of the airplane.

The presence of wing interference effects on the floating characteristics of the rudders is indicated by comparing figure 7 (wing removed) with figure 5 (complete model). At angles of attack of 15° and 25°,

the addition of the wing resulted in the plain and the horn-balanced rudders' floating at deflections that were more with the spin than those obtained with the wing removed, and for the angle-of-attack range from 35° to 55° both rudders oscillated violently. A study of the tuft pictures for angles of attack of 35° and 45° showed that the presence of the wing resulted in turbulent flow in the region of the vertical tail and indicated that the wake of the stalled wing blanketed the tail and caused the erratic oscillatory motions of the rudders. At an angle of attack of 65°, the floating angles were steady and approximately the same floating angles were obtained for the configurations with the wing on and off; this fact indicates that the tail was not in the wake of the wing for this angle of attack.

Spin Recovery with Controls Released

As indicated previously, reference 3 gave some indications of the deflections to which the rudder must float for satisfactory recovery with controls released. The rudder position and other control positions required for satisfactory recovery were shown to be dependent upon the center-of-gravity position, the loading, and the amount of tail damping of the airplane. In general, ailerons tend to float with the spin as indicated in reference 8 and unpublished results, and elevators tend to float at up deflections (reference 1) after control release from spinning attitudes. Reference 3 indicated that for these aileron and elevator deflections the rudder should float to large deflections against the spin in order to obtain recoveries from spins with controls released. The rudder-deflection requirement, however, was not fulfilled by the plain or horn-balanced rudder on the low-wing airplane configuration investigated herein. For a high-wing configuration, the angle-of-attack range for which wing interference is obtained may be decreased, but even without wing interference the horn-balanced rudder would not fulfill the rudder-deflection requirement for recovery with elevators up and ailerons with the spin. Some device therefore seems to be necessary for movement of the elevators or ailerons to a position for which the requirement of rudder floating deflections for recovery would be less stringent.

Comparison of Rudder Floating Angles Determined from Static and from Rotary Tests

In order to compare floating angles predicted by static data with those obtained from rotary tests, an analysis of available comparable data was made. This comparison could be made only for the isolated vertical tail and the vertical tail in the presence of a horizontal tail.

The curves presented in figure 6 for the plain rudder with wing and horizontal tail removed are compared in figure 12 with curves obtained from static hinge-moment data presented in reference 6 for a plain rudder on an isolated vertical tail. This figure shows that for the rotary data the rudder floated at neutral for 0° sideslip except at an angle of attack of 15° and that the floating angles obtained during rotary tests and the floating angles determined from static tests were generally in good agreement except at an angle of attack of 15°. For a large spinning angle-of-attack range, the sideslip value at the arbitrary reference point on the rudder (point chosen for calculating sideslip at tail for rotary tests) was therefore approximately equal to the effective sideslip over the tail.

Curves for angles of attack of 15°, 25°, and 35° (presented in fig. 7) for the plain rudder with only the wing removed are compared in figure 13 with curves obtained from static hinge-moment data presented in reference 6 for a plain rudder on a vertical tail in the presence of only a horizontal tail having a low and a high position on the vertical tail. Although a discrepancy between floating angles determined from rotary and static tests was obtained only at an angle of attack of 15° when the horizontal tail was removed, figure 13 indicates that, in the presence of a horizontal tail, discrepancies between the floating angles existed throughout the angle-of-attack range presented. The rudder during rotary tests floated at deflections which were less with the spin than those obtained during static tests. It was mentioned previously that reference 7 showed that during rotary tests the negative pressure over the upper surface of the horizontal tail is greater on the outboard side than on the inboard side of the horizontal tail and the rudder area shielded by the horizontal tail lies in this differential-pressure region. It was also shown in reference 7 that this differential pressure does not exist during static tests and that this differential pressure during rotation, therefore, was due to a variation of angle of attack along the span of the horizontal tail. Since this differential pressure creates a moment which tends to move the rudder in a direction which is less with the spin and because this differential pressure due to rotation is not present during static tests, it would be expected, as is shown in figure 13, that in rotary tests the rudders would float at deflections which are less with the spin than those obtained in static tests. Rudder floating characteristics for static and rotary tests, therefore, will differ when horizontal-tail interference is present. The hinge moments presented in reference 6 for the plain rudder in the presence of a horizontal tail became very small above an angle of attack of 30° because of the shielding of the horizontal tail, and the floating characteristics were irregular and inconclusive. The comparison between floating angles determined from rotary and static tests was, therefore, not extended beyond an angle of attack of 35°.

CONCLUSIONS

The following conclusions are based on floating angles obtained at spinning attitudes during rotary tests on full-length plain and horn-balanced rudders on a $\frac{1}{6}$-scale model of a typical low-wing personal-owner airplane:

1. The horn-balanced rudder had more desirable floating characteristics than the plain rudder for low spinning angles of attack (15° to 25°), and at higher spinning angles of attack (35° to 55°) both rudders were in the wake of the stalled wing and oscillated violently.

2. Neither rudder would fulfill the rudder-deflection requirement for satisfactory spin recovery with the type of aileron and elevator deflections that are present with controls released.

3. With no wing interference, the horn-balanced rudder generally would have more favorable floating characteristics than the plain rudder through a large angle-of-attack range for a normal sideslip-angle range.

4. Horizonal-tail interference led to an appreciable difference between floating angles obtained from static data and from rotary data.

Langley Aeronautical Laboratory
National Advisory Committee for Aeronautics
Langley Field, Va., February 12, 1951

REFERENCES

1. Bihrle, William, Jr.: Floating Characteristics of Rudders and Elevators in Spinning Attitudes as Determined from Hinge-Moment-Coefficient Data with Application to Personal-Owner-Type Airplanes. NACA TN 2016, 1950.

2. Anon.: Airplane Airworthiness - Normal, Utility, Acrobatic, and Restricted Purpose Categories. Pt. 03 of Civil Air Regulations, Civil Aero. Board, U. S. Dept. Commerce, Dec. 15, 1946, pp. 11-12, secs. 03.135-N - 03.135-A.

3. Klinar, Walter J., and Wilson, Jack H.: A Spin-Tunnel Investigation of the Effects of Mass and Dimensional Variations on the Spinning Characteristics of a Low-Wing Single-Vertical-Tail Model Typical of Personal-Owner Airplanes. NACA TN 2352, 1951.

4. Lowry, John G.: Résumé of Hinge-Moment Data for Unshielded Horn-Balanced Control Surfaces. NACA RB 3F19, 1943.

5. Stone, Ralph W., Jr., Burk, Sanger M., Jr., and Bihrle, William, Jr.: The Aerodynamic Forces and Moments on a $\frac{1}{10}$-Scale Model of a Fighter Airplane in Spinning Attitudes as Measured on a Rotary Balance in the Langley 20-Foot Free-Spinning Tunnel. NACA TN 2181, 1950.

6. Stone, Ralph W., Jr., and Burk, Sanger M., Jr.: Effect of Horizontal-Tail Position on the Hinge Moments of an Unbalanced Rudder in Attitudes Simulating Spin Conditions. NACA TN 1337, 1947.

7. Kohler, M., and Mautz, W.: Pressure-Distribution Measurements on the Tail Surfaces of a Rotating Model of the Design BFW - M 31. NACA TM 1220, 1949.

8. Stone, Ralph W., Jr., and Schneiter, Leslie E.: Calculation of the Aileron and Elevator Stick Forces and Rudder Pedal Forces for the Bell XP-83 Airplane (Project MX-511) in Spins. NACA MR L5H29, 1945.

TABLE I.- DIMENSIONAL CHARACTERISTICS OF THE SIMULATED FULL-SCALE AIRPLANE

Length, over-all, ft	22.40
Wing:	
Span, ft	33.63
Area, sq ft	163.4
Section	NACA 23012
Twist, deg	0
Incidence, deg	3
Dihedral, deg	6
Mean aerodynamic chord, ft	4.89
Distance of leading edge of mean aerodynamic chord rearward of leading edge of wing, ft	0.05
Taper ratio	1.00
Aspect ratio	6.93
Ailerons:	
Span, ft	7.19
Area rearward of hinge line, sq ft	15.70
Aspect ratio	6.58
Horizontal tail surface:	
Span, ft	10.25
Total area, sq ft	26.39
Elevator area rearward of hinge line, sq ft	11.02
Aspect ratio	3.98
Incidence, deg	0
Dihedral, deg	0
Distance from quarter chord of mean aerodynamic chord to elevator hinge line, ft	13.73
Section	NACA 0009
Vertical tail surface:	
Total area, sq ft	12.96
Total unbalanced rudder area, rearward of hinge line, sq ft	6.48
Aspect ratio	1.26
Offset, deg	0
Rudder height along hinge line, ft	5.32
Distance from quarter chord of mean aerodynamic chord to rudder hinge line, ft	14.17
Section	NACA 0009

TABLE II.- CONDITIONS TESTED FOR ALL CONFIGURATIONS

[Full-scale values given]

α (deg)	Test	ϕ (deg)	β_{cg} (deg)	β_t (deg)	R_s (ft)	Ω (rps)	V (fps)
15	1	-12	-18.0	-19.1	3.5	0.65	136
	2	-8	-14.0	-16.6			
	3	-4	-10.0	-13.4			
	4	0	-6.0	-9.6			
	5	4	-2.0	-5.4			
	6	8	2.0	-.6			
	7	12	6.0	4.9			
	8	-12	-19.7	-20.5	6.0	0.45	126
	9	-8	-15.7	-17.7			
	10	-4	-11.7	-14.2			
	11	0	-7.7	-10.3			
	12	4	-3.7	-6.2			
	13	8	.3	-1.7			
	14	12	4.3	3.5			
25	15	-16	-31.1	-34.8	12.0	0.45	126
	16	-12	-27.1	-31.6			
	17	-8	-23.1	-28.0			
	18	-4	-19.1	-24.3			
	19	0	-15.1	-20.4			
	20	4	-11.1	-16.3			
	21	8	-7.1	-12.0			
	22	12	-3.1	-7.6			
	23	16	.9	-2.8			
	24	-16	-26.2	-28.8	12.0	0.30	126
	25	-12	-22.2	-25.3			
	26	-8	-18.2	-21.7			
	27	-4	-14.2	-17.8			
	28	0	-10.2	-13.9			
	29	4	-6.2	-9.8			
	30	8	-2.2	-5.7			
	31	12	1.8	-1.3			
	32	16	5.8	3.2			
	33	-16	-22.9	-24.6	12.0	0.23	144
	34	-12	-18.9	-21.0			
	35	-8	-14.9	-17.2			
	36	-4	-10.9	-13.3			
	37	0	-6.9	-9.4			
	38	4	-2.9	-5.3			
	39	8	1.1	-1.2			
	40	12	5.1	3.0			
	41	16	9.1	7.4			
35	42	-16	-31.1	-37.9	12.0	0.45	126
	43	-12	-27.1	-34.3			
	44	-8	-23.1	-30.6			
	45	-4	-19.1	-26.8			
	46	0	-15.1	-22.9			
	47	4	-11.1	-18.8			
	48	8	-7.1	-14.6			
	49	12	-3.1	-10.3			
	50	16	.9	-5.9			
	51	-16	-26.2	-31.0	12.0	0.30	126
	52	-12	-22.2	-27.3			
	53	-8	-18.2	-23.5			
	54	-4	-14.2	-19.7			
	55	0	-10.2	-15.7			
	56	4	-6.2	-11.7			
	57	8	-2.2	-7.5			
	58	12	1.8	-3.3			
	59	16	5.8	1.0			
	60	-16	-22.9	-26.1	12.0	0.23	144
	61	-12	-18.9	-22.3			
	62	-8	-14.9	-18.5			
	63	-4	-10.9	-14.6			
	64	0	-6.9	-10.6			
	65	4	-2.9	-6.6			
	66	8	1.1	-2.5			
	67	12	5.1	1.7			
	68	16	9.1	5.9			

α (deg)	Test	ϕ (deg)	β_{cg} (deg)	β_t (deg)	R_s (ft)	Ω (rps)	V (fps)
45	69	-16	-31.1	-40.2	12.0	0.45	126
	70	-12	-27.1	-36.6			
	71	-8	-23.1	-32.9			
	72	-4	-19.1	-29.0			
	73	0	-15.1	-25.1			
	74	4	-11.1	-21.0			
	75	8	-7.1	-16.9			
	76	12	-3.1	-12.6			
	77	16	.9	-8.2			
	78	-16	-26.2	-32.7	12.0	0.30	126
	79	-12	-22.2	-29.0			
	80	-8	-18.2	-25.2			
	81	-4	-14.2	-21.3			
	82	0	-10.2	-17.3			
	83	4	-6.2	-13.3			
	84	8	-2.2	-9.2			
	85	12	1.8	-5.0			
	86	16	5.8	-.7			
	87	-16	-22.9	-27.3	12.0	0.23	144
	88	-12	-18.9	-23.5			
	89	-8	-14.9	-19.6			
	90	-4	-10.9	-15.7			
	91	0	-6.9	-11.8			
	92	4	-2.9	-7.7			
	93	8	1.1	-3.6			
	94	12	5.1	.5			
	95	16	9.1	4.7			
55	96	-16	-22.0	-38.2	3.5	0.56	117
	97	-12	-18.0	-34.5			
	98	-8	-14.0	-30.7			
	99	-4	-10.0	-26.9			
	100	0	-6.0	-22.9			
	101	4	-2.0	-18.9			
	102	8	2.0	-14.7			
	103	12	6.0	-10.5			
	104	16	10.0	-6.2			
	105	-16	-24.5	-31.1	12.0	0.23	116
	106	-12	-20.5	-27.4			
	107	-8	-16.5	-23.6			
	108	-4	-12.5	-19.7			
	109	0	-8.5	-15.8			
	110	4	-4.5	-11.7			
	111	8	-.5	-7.6			
	112	12	3.5	-3.4			
	113	16	7.5	.9			
65	114	-16	-17.3	-45.1	0.5	0.56	78
	115	-12	-13.3	-41.2			
	116	-8	-9.3	-37.4			
	117	-4	-5.3	-33.4			
	118	0	-1.3	-29.5			
	119	4	2.7	-25.4			
	120	8	6.7	-21.4			
	121	12	10.7	-17.2			
	122	16	14.7	-13.1			
	123	-16	-21.7	-37.1	4.0	0.45	113
	124	-12	-17.7	-33.4			
	125	-8	-13.7	-29.6			
	126	-4	-9.7	-25.8			
	127	0	-5.7	-21.9			
	128	4	-1.7	-17.8			
	129	8	2.3	-13.6			
	130	12	6.3	-9.4			
	131	16	10.3	-5.1			

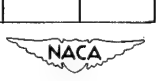

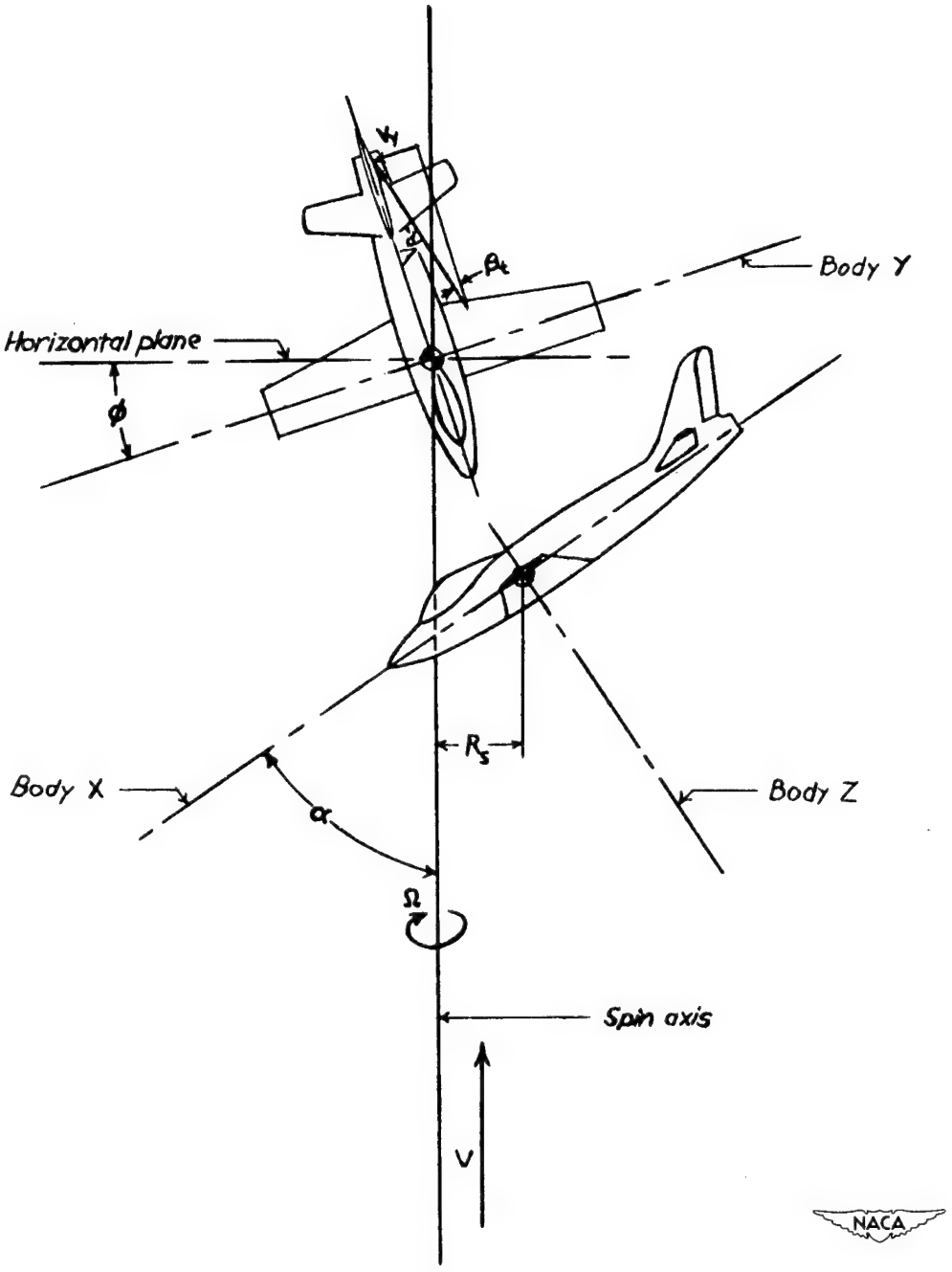

Figure 1.- Illustration of the angles, velocities, and spin radius as measured on an airplane in a right spin. Body axes are also shown.

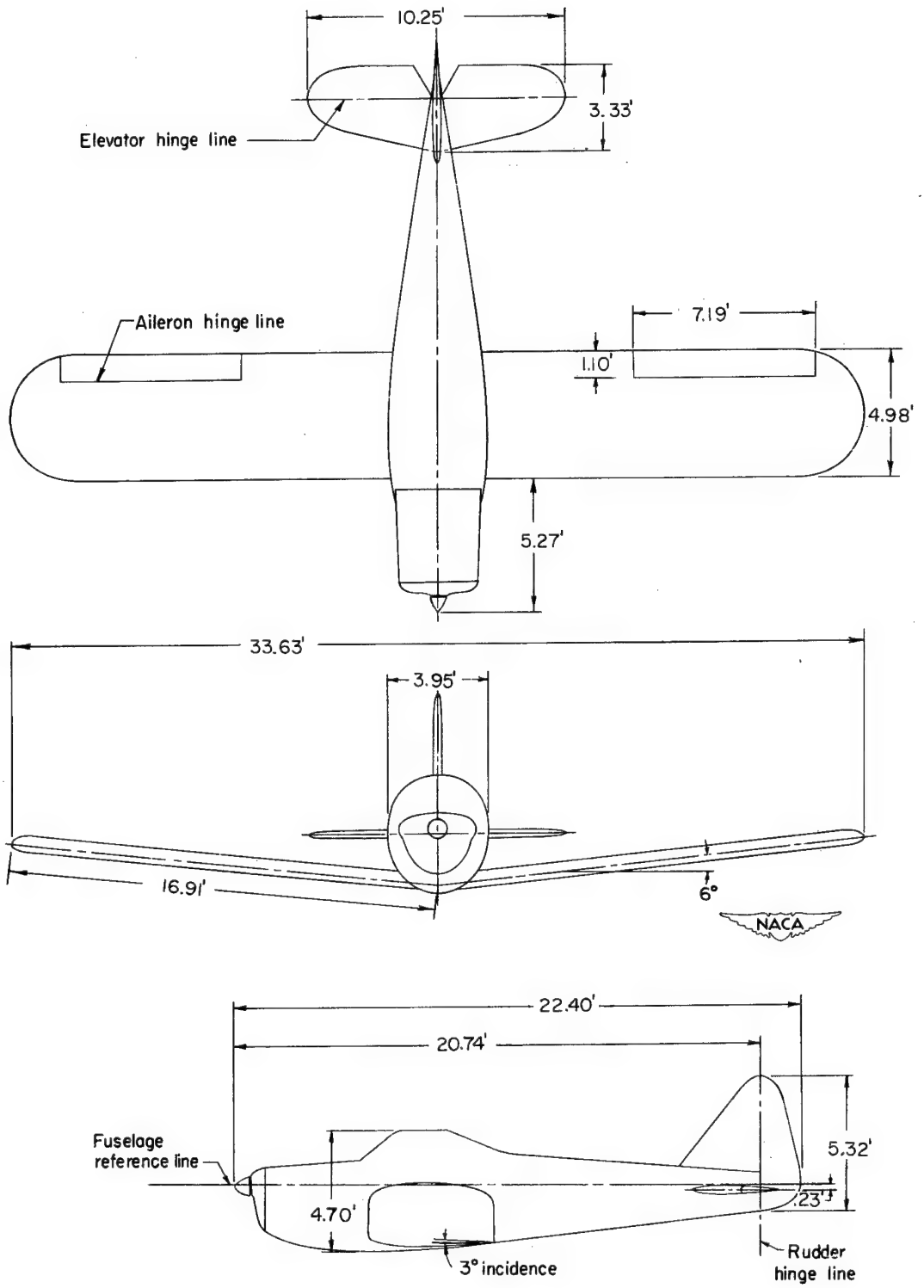

Figure 2.- Three-view drawing of the typical personal-owner airplane simulated by the $\frac{1}{6}$ - scale model.

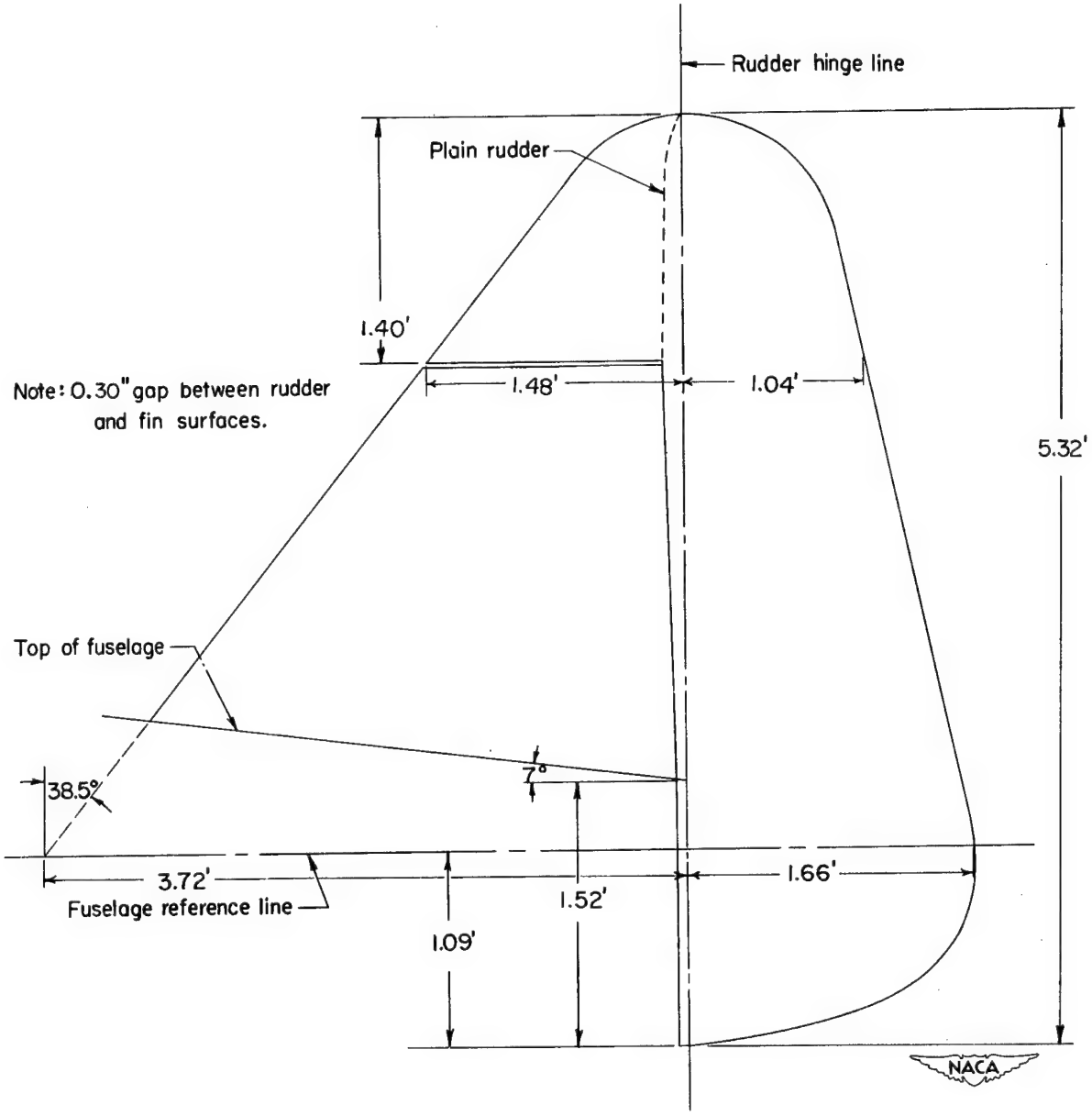

Figure 3.- Sketch of the vertical tail with the plain and with the horn-balanced rudder.

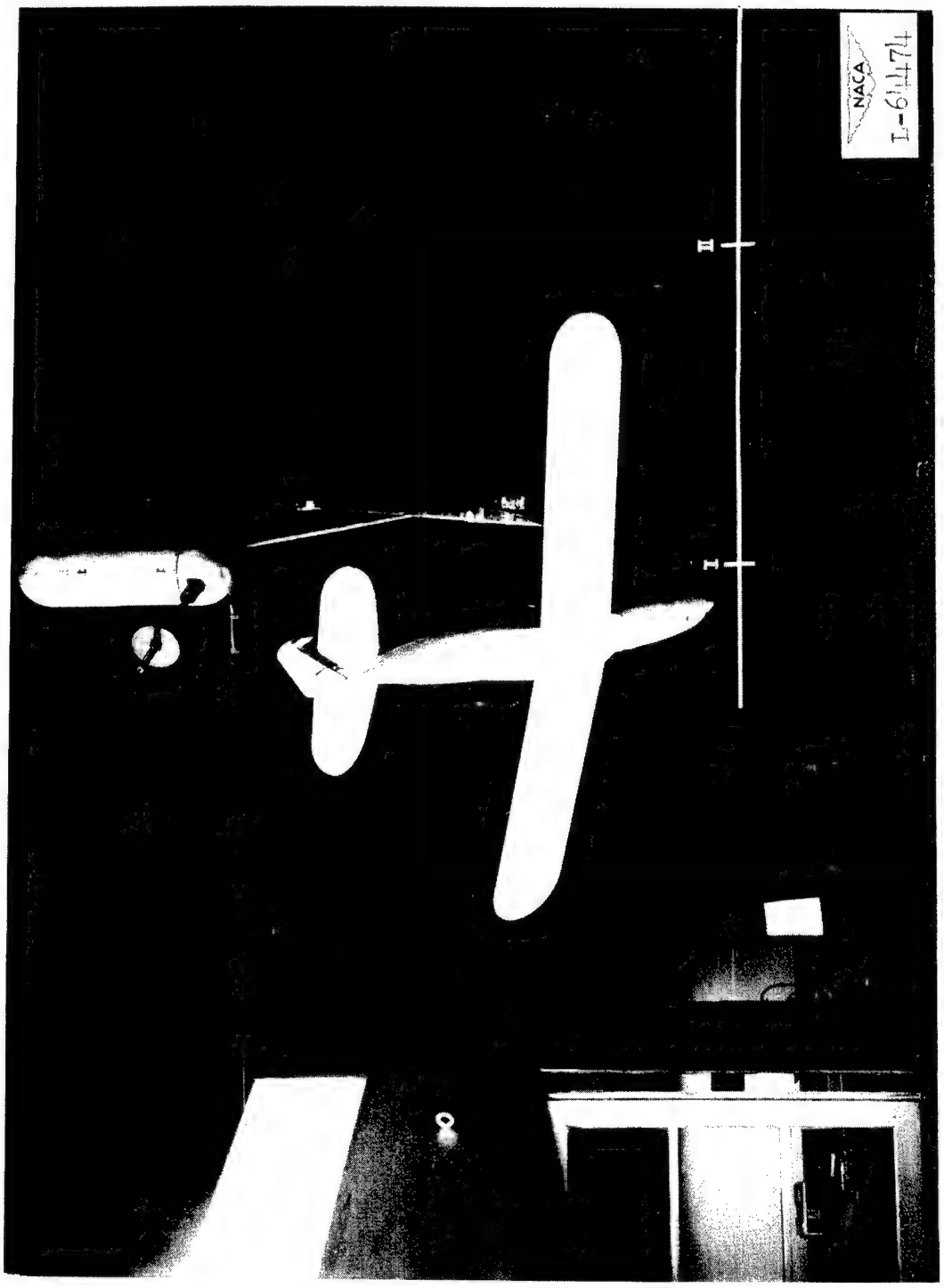

Figure 4.- Photograph of the model mounted on the rotary balance.

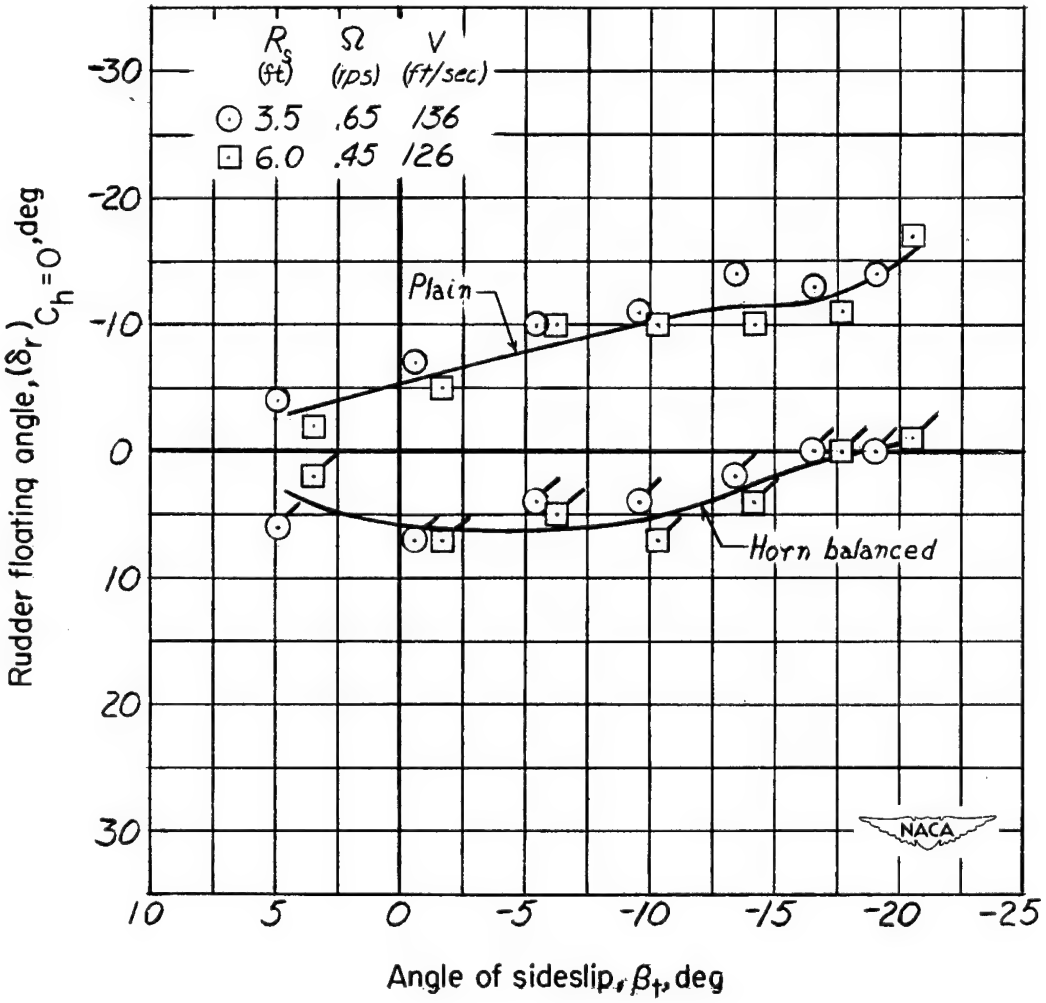

(a) $\alpha = 15^\circ$.

Figure 5.- Plain-rudder and horn-balanced-rudder floating angles for complete model configuration as a function of sideslip at the tail for specific angles of attack. (Unflagged symbols denote plain rudder; flagged symbols denote horn-balanced rudder. Plotting of test data is discontinued after the rudder attained a full-with-the-spin deflection. For test points where floating angles were oscillatory, the range of oscillation is indicated.)

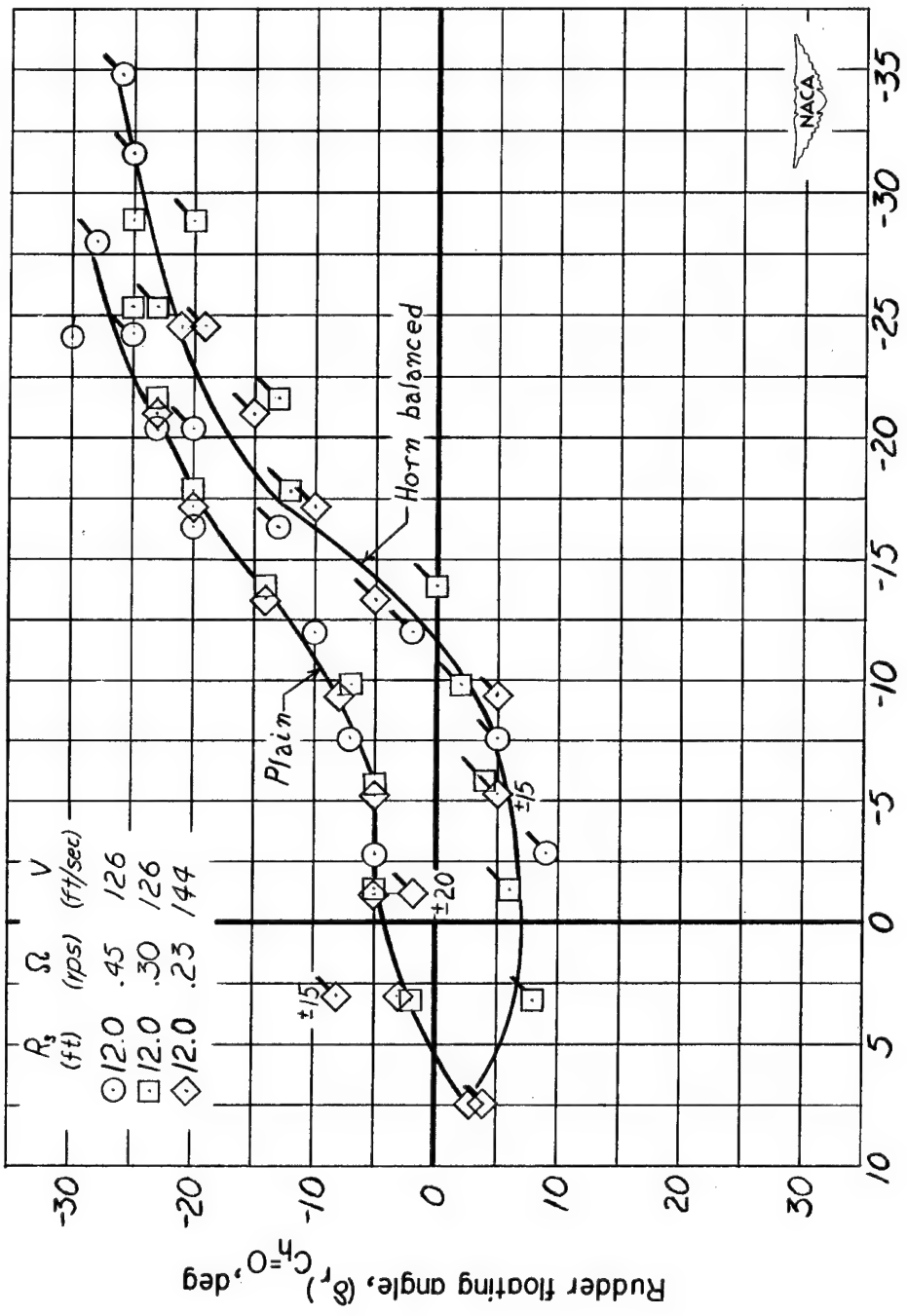

(b) $\alpha = 25^\circ$.

Figure 5.- Continued.

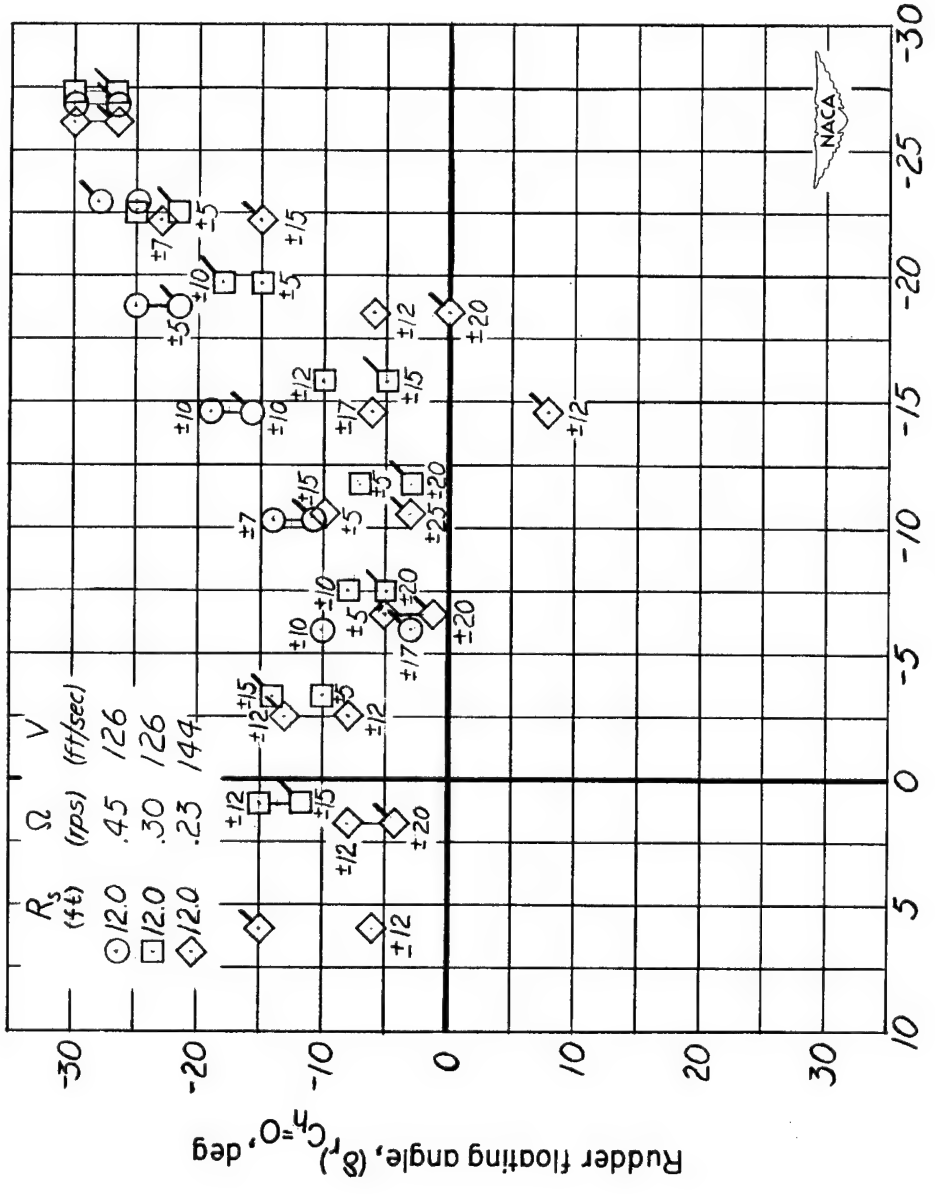

(c) $\alpha = 35°$.

Figure 5.- Continued.

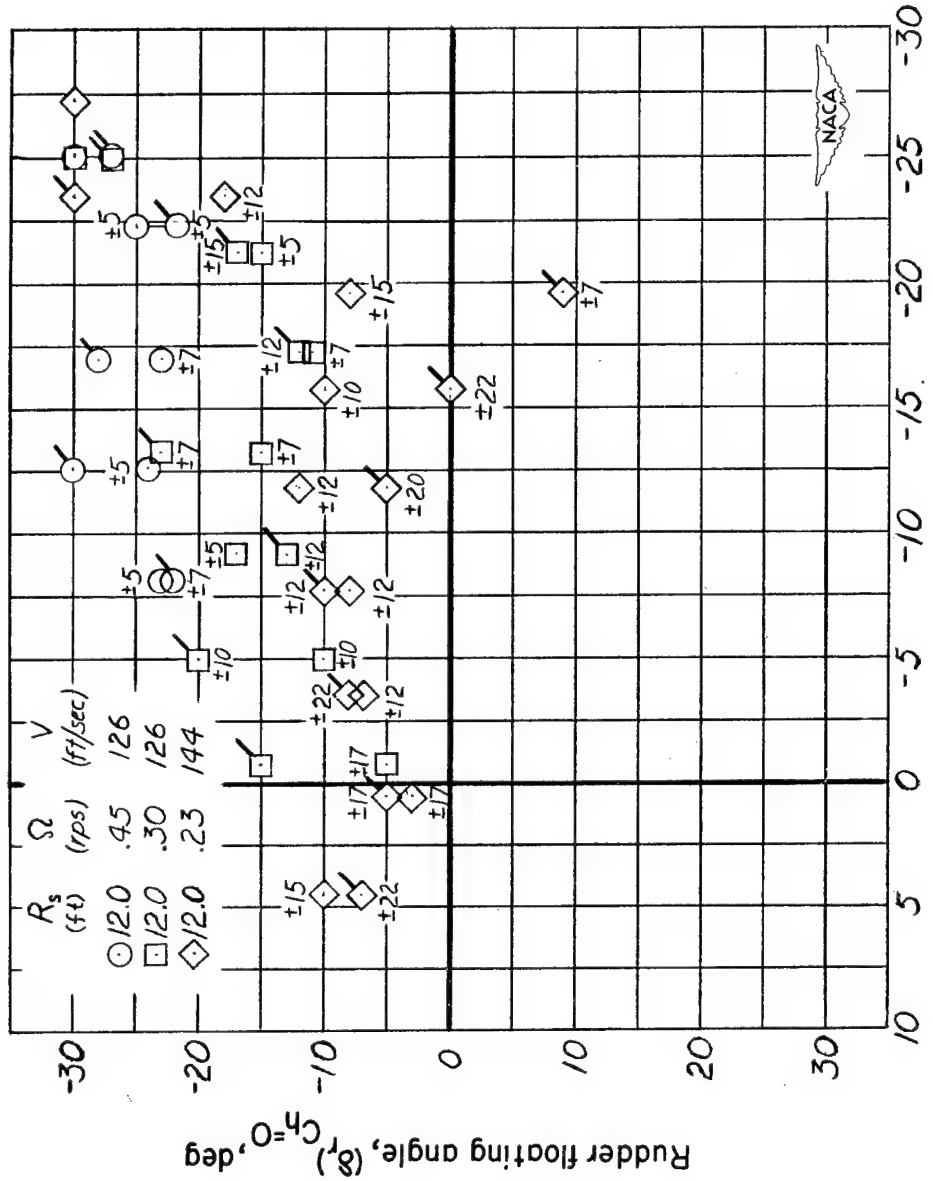

(d) $\alpha = 45°$.

Figure 5.- Continued.

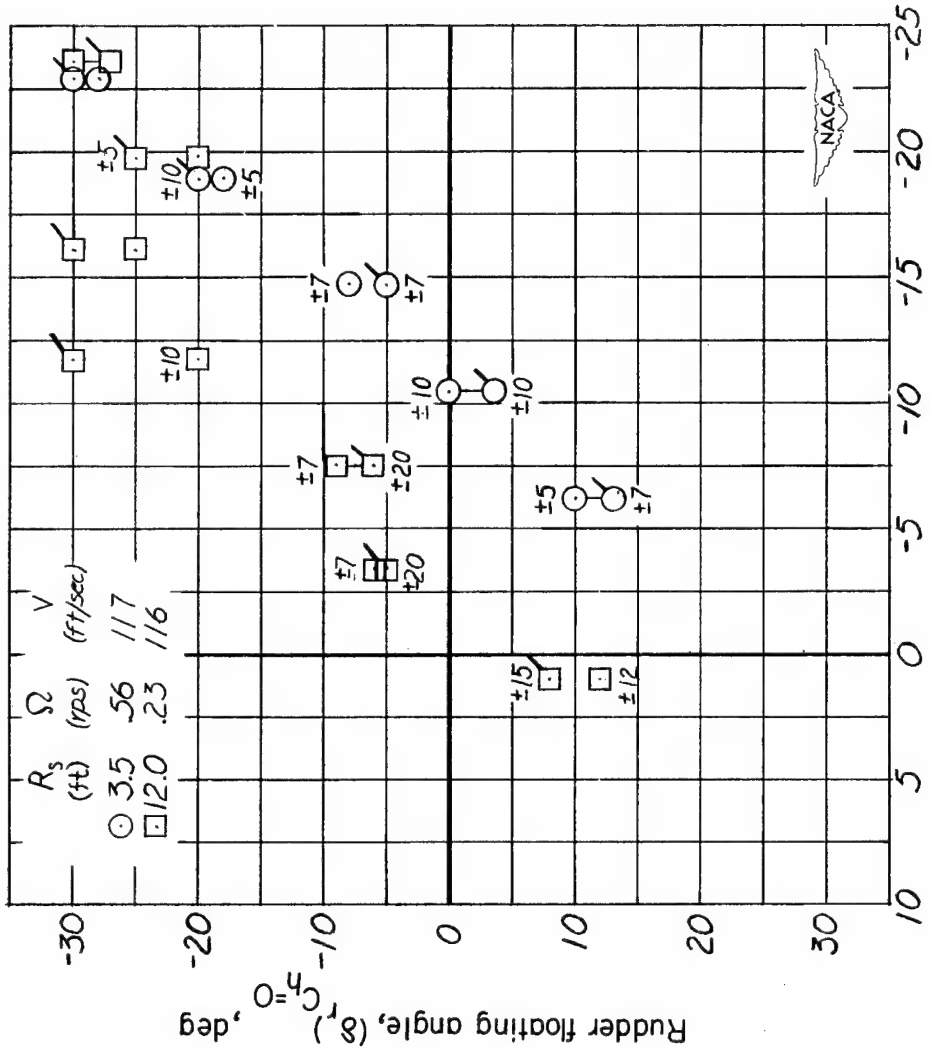

(e) $\alpha = 55^\circ$.

Figure 5.- Continued.

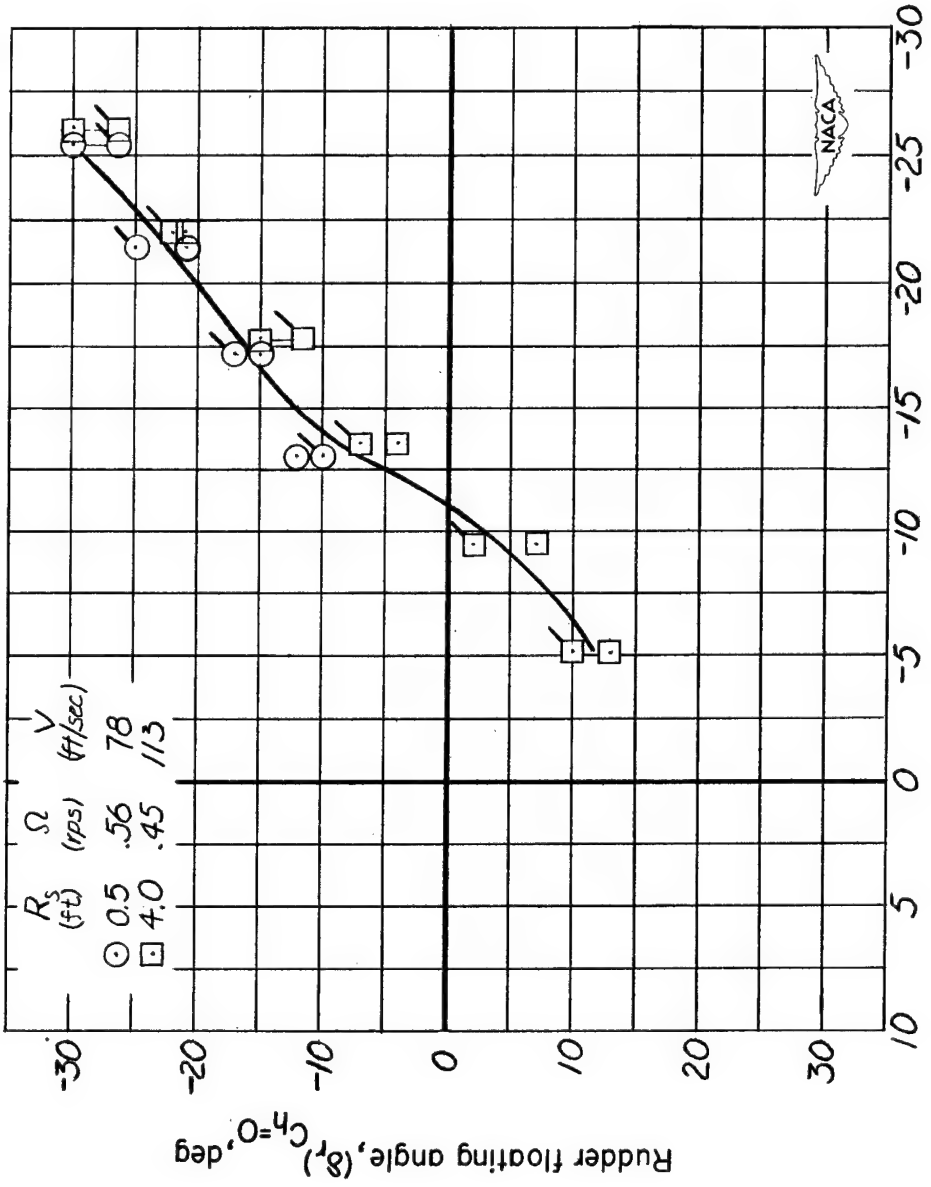

(f) $\alpha = 65^\circ$.

Figure 5.- Concluded.

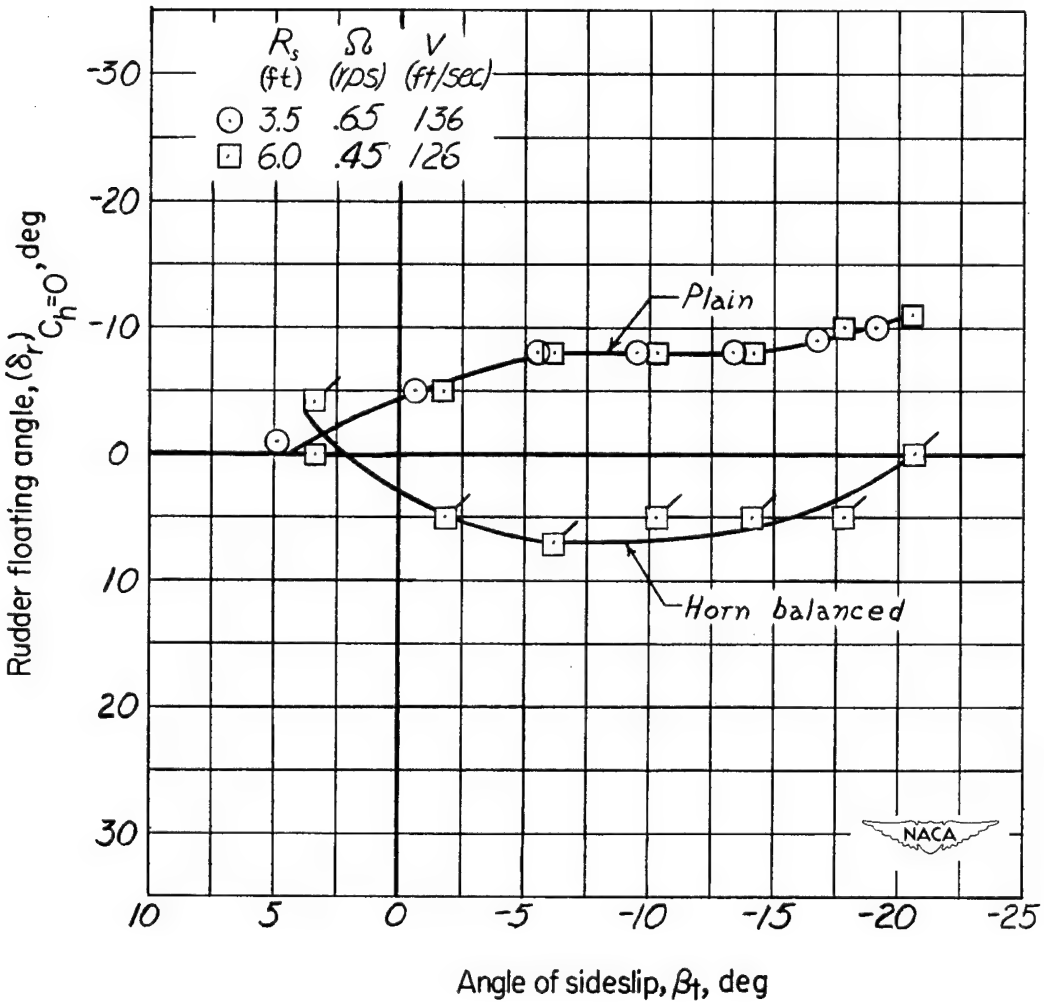

(a) $\alpha = 15^\circ$.

Figure 6.- Plain-rudder and horn-balanced-rudder floating angles for configuration with horizontal tail and wing removed as a function of sideslip at the tail for specific angles of attack. (Unflagged symbols denote plain rudder; flagged symbols denote horn-balanced rudder. Plotting of test data is discontinued after the rudder attained a full-with-the-spin deflection. For test points where floating angles were oscillatory, the range of oscillation is indicated.)

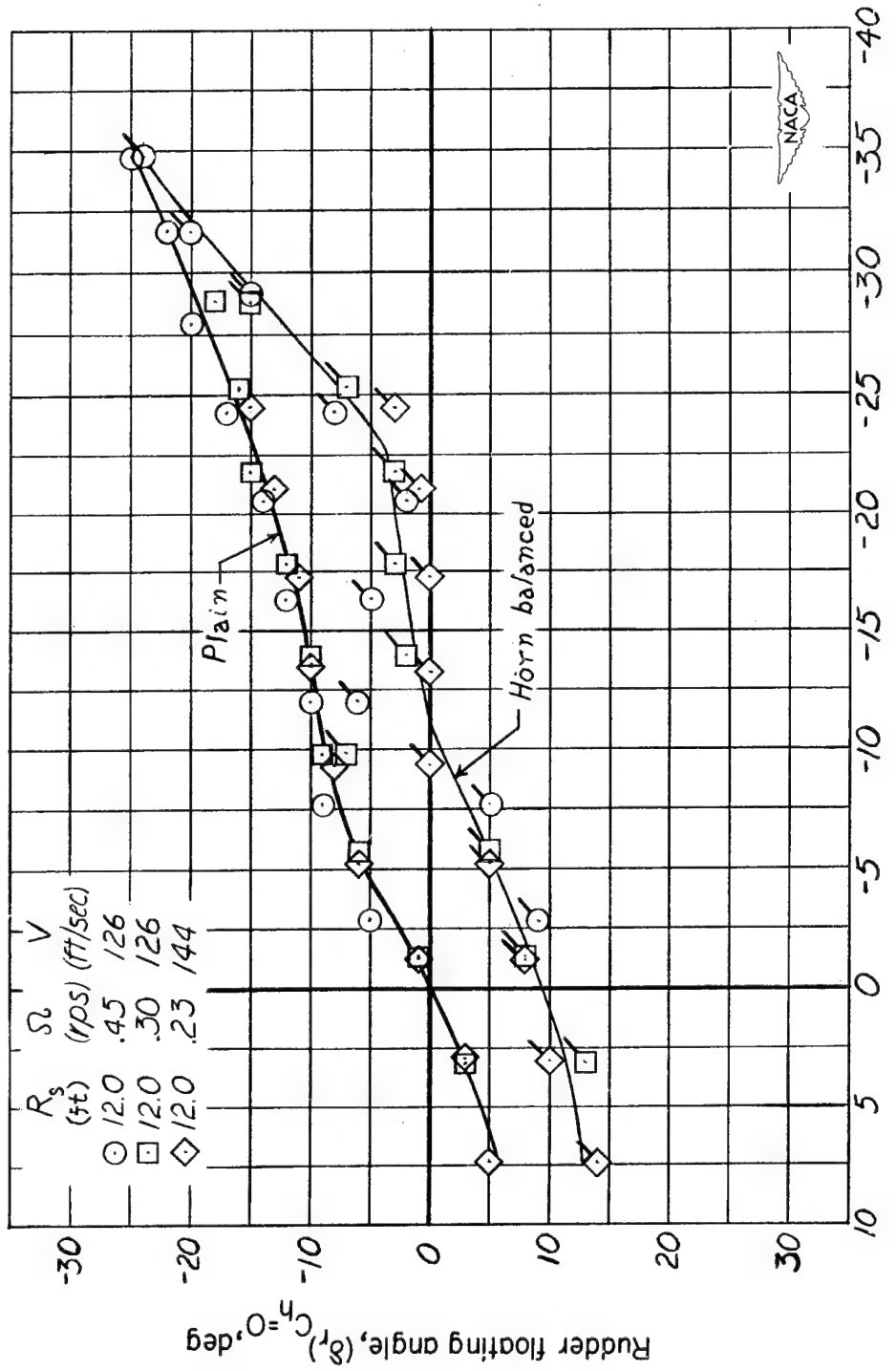

(b) $\alpha = 25°$.

Figure 6.- Continued.

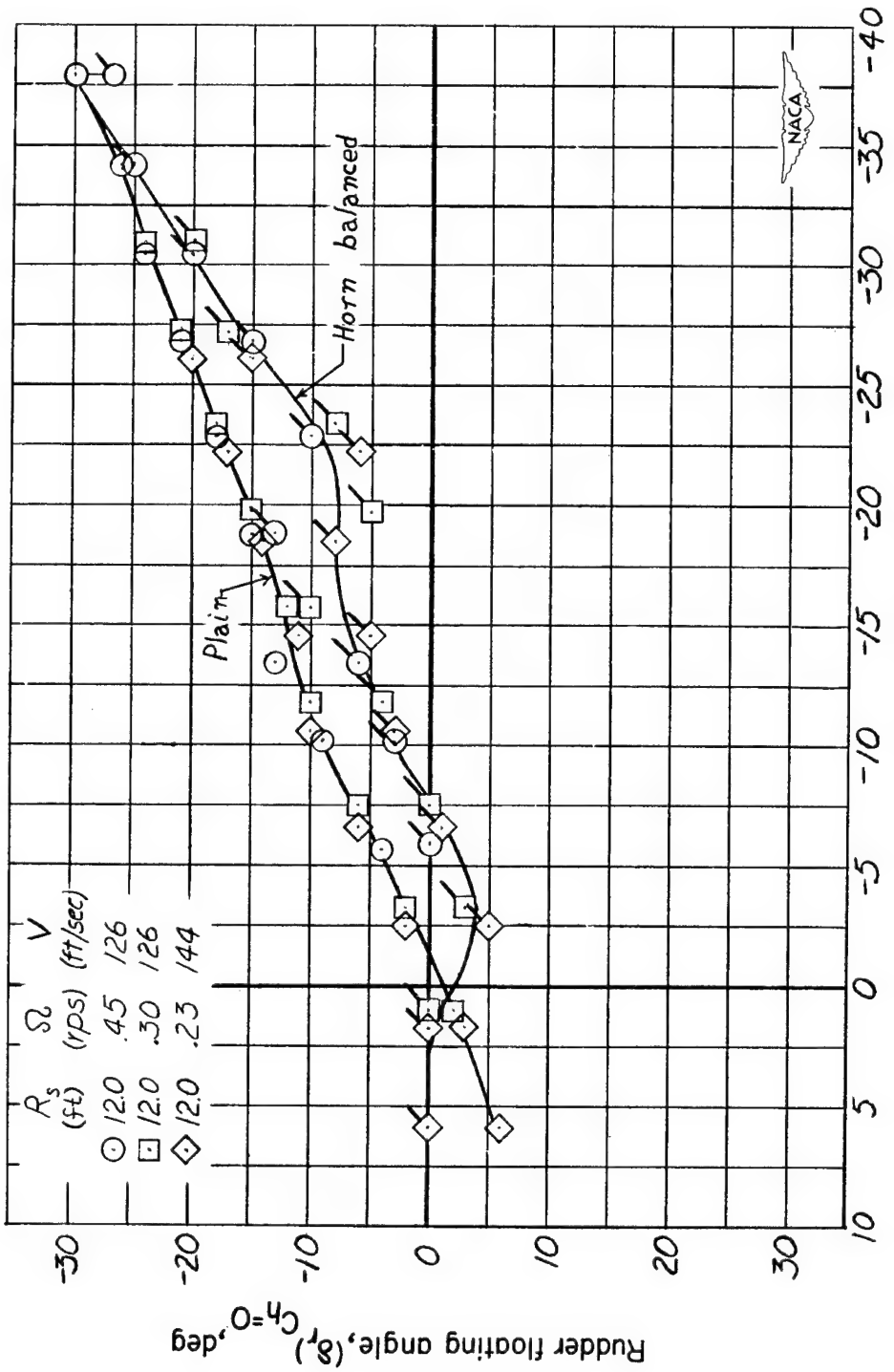

(c) $\alpha = 35°$.

Figure 6.- Continued.

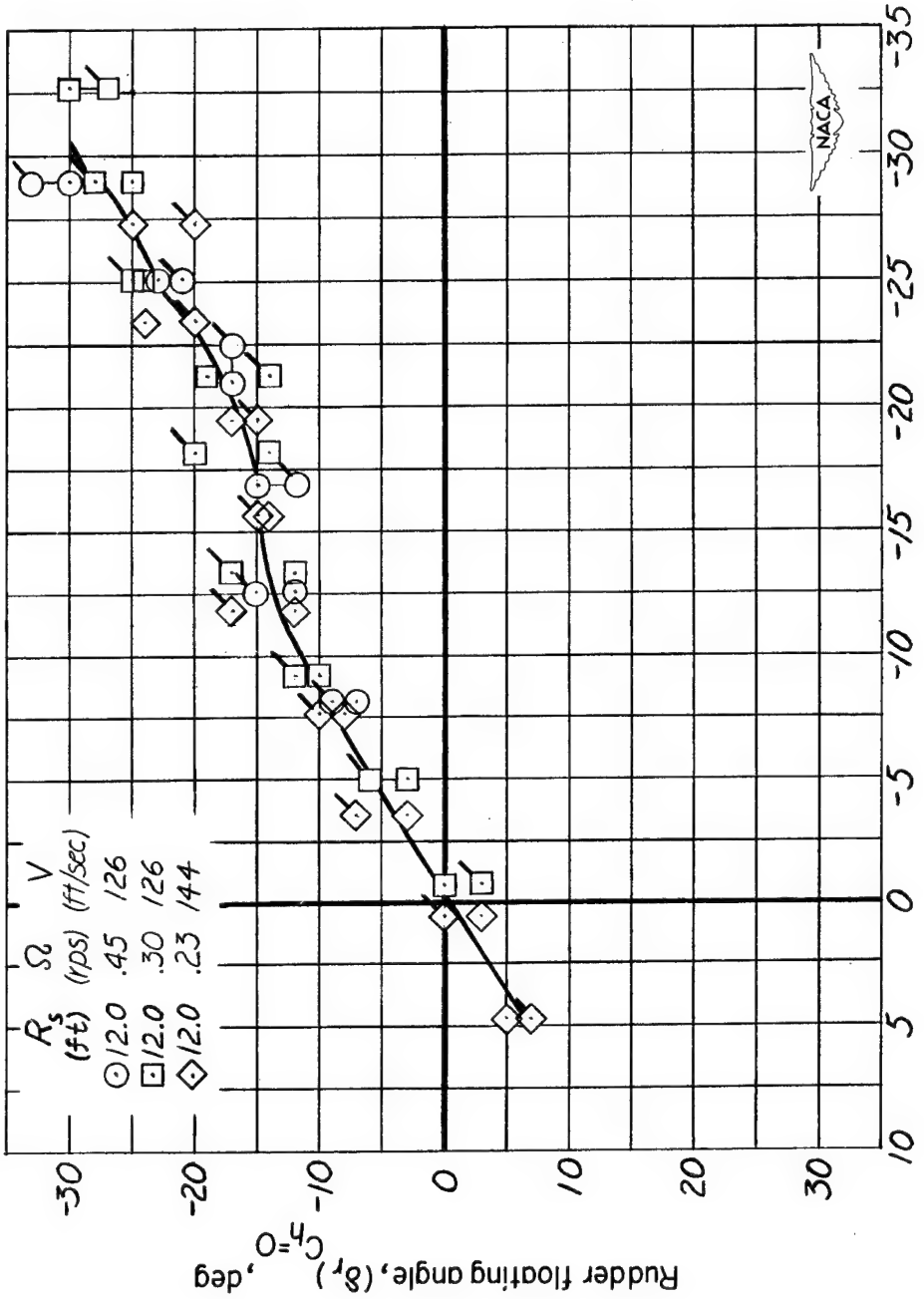

(d) $\alpha = 45°$.

Figure 6.- Continued.

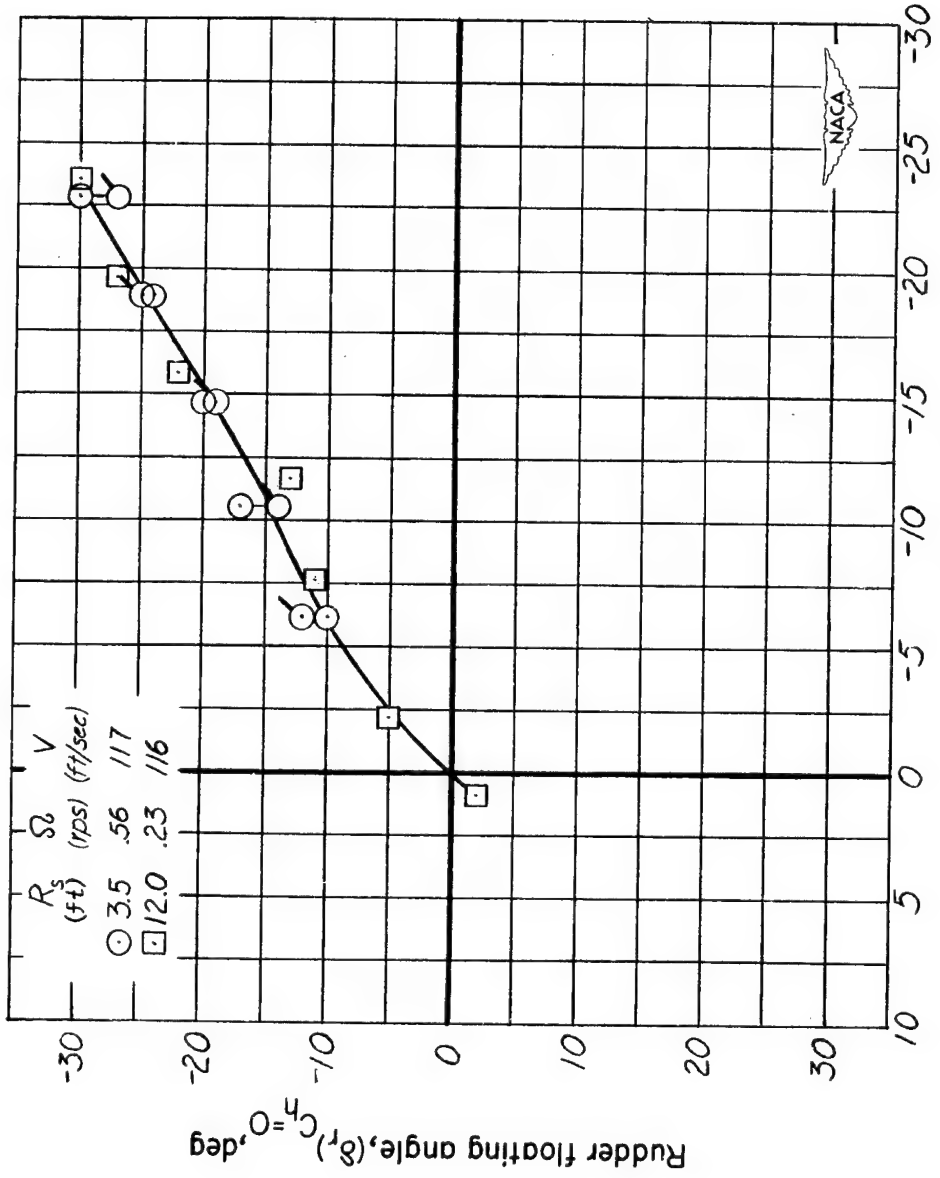

(e) $\alpha = 55^\circ$.

Figure 6.- Continued.

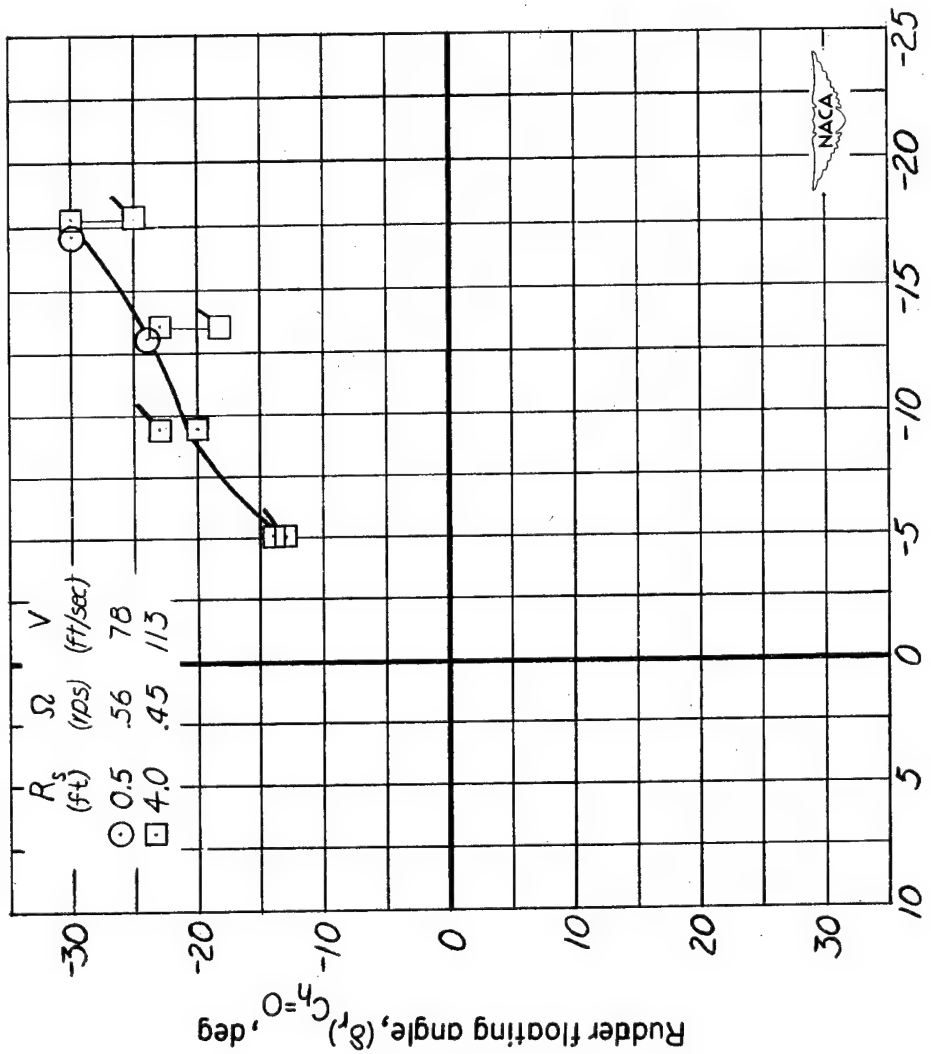

(f) $\alpha = 65°$.

Figure 6.- Concluded.

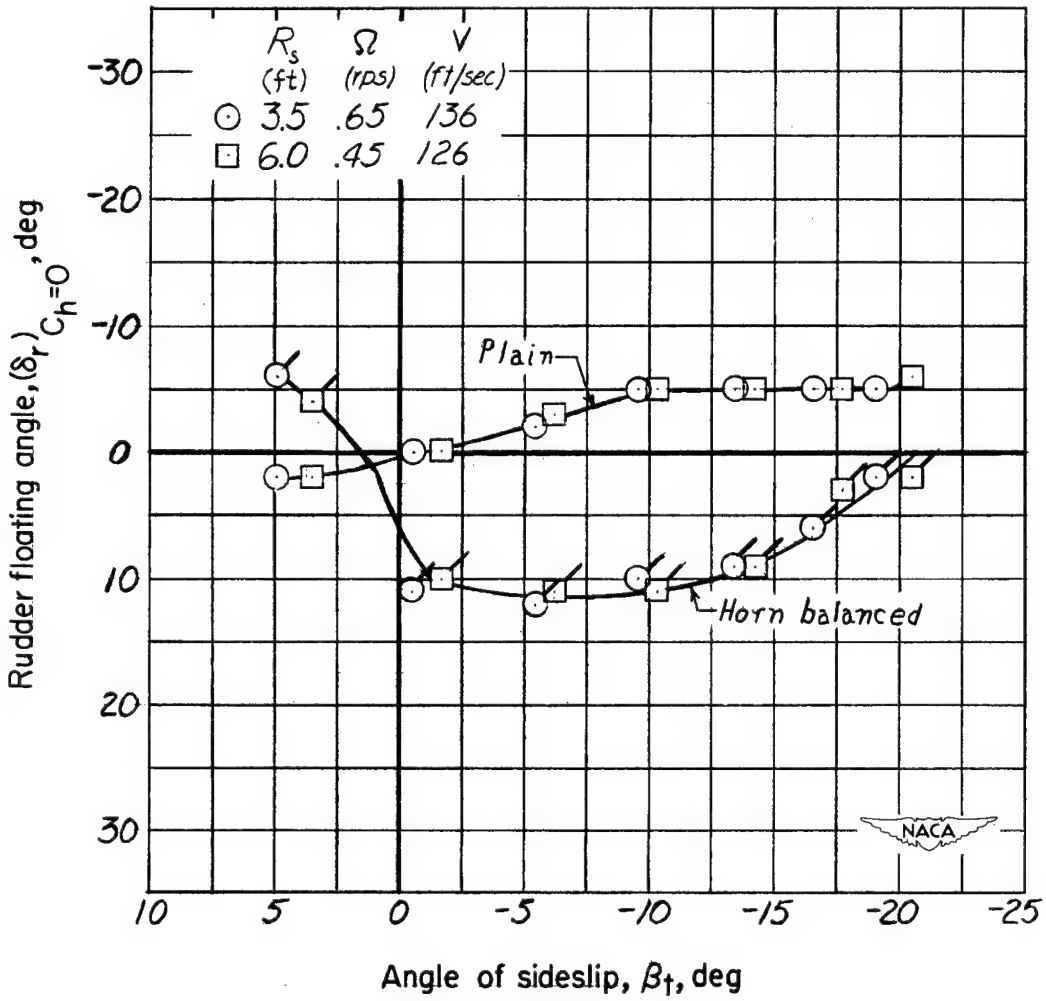

(a) $\alpha = 15^\circ$.

Figure 7.- Plain-rudder and horn-balanced-rudder floating angles for configuration with wing removed as a function of sideslip at the tail for specific angles of attack. (Unflagged symbols denote plain rudder; flagged symbols denote horn-balanced rudder. Plotting of test data is discontinued after the rudder attained a full-with-the-spin deflection. For test points where floating angles were oscillatory, the range of oscillation is indicated.)

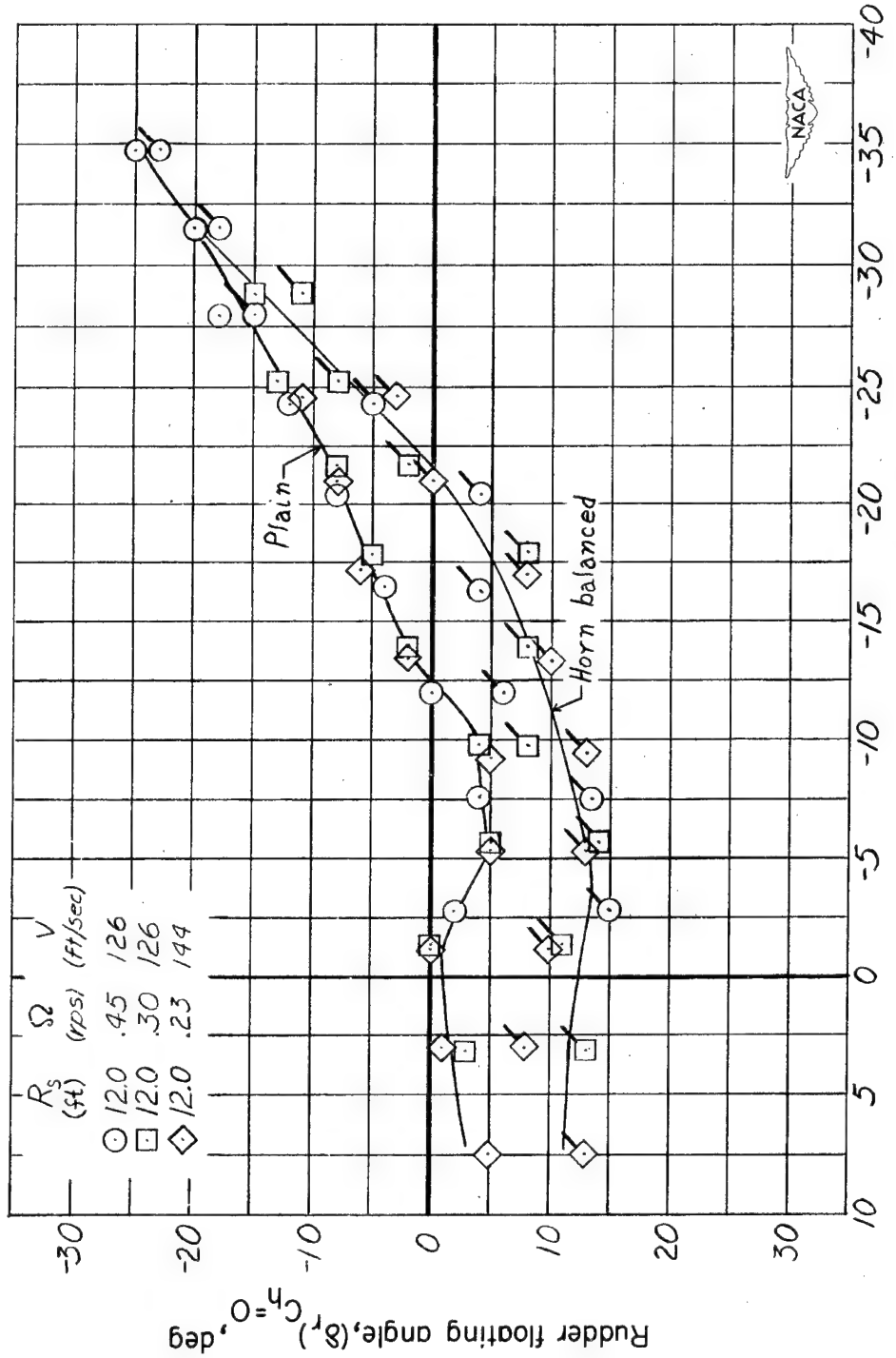

(b) $\alpha = 25°$.

Figure 7.- Continued.

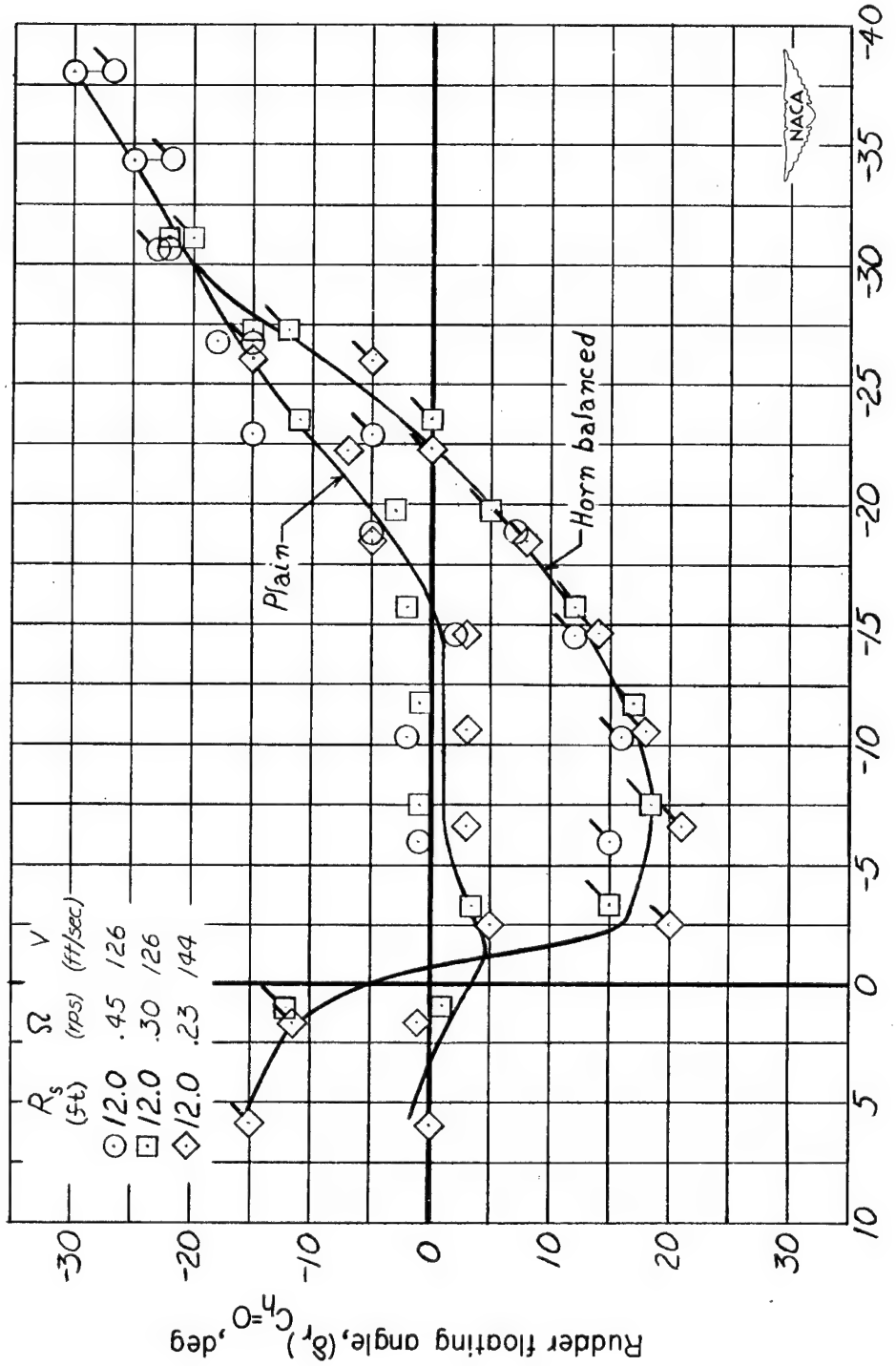

(c) $\alpha = 35^\circ$.

Figure 7.- Continued.

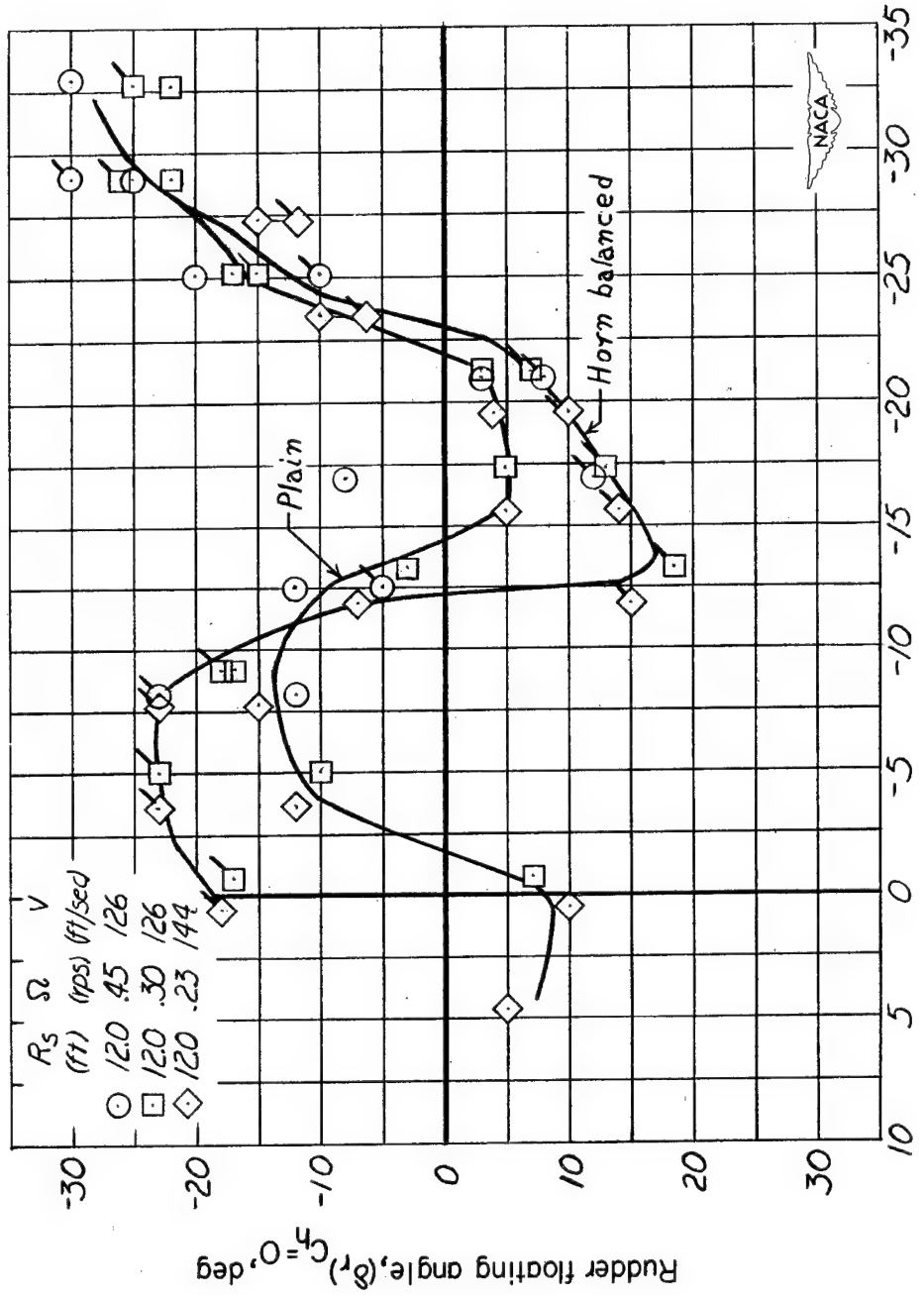

(d) $\alpha = 45^\circ$.

Figure 7.- Continued.

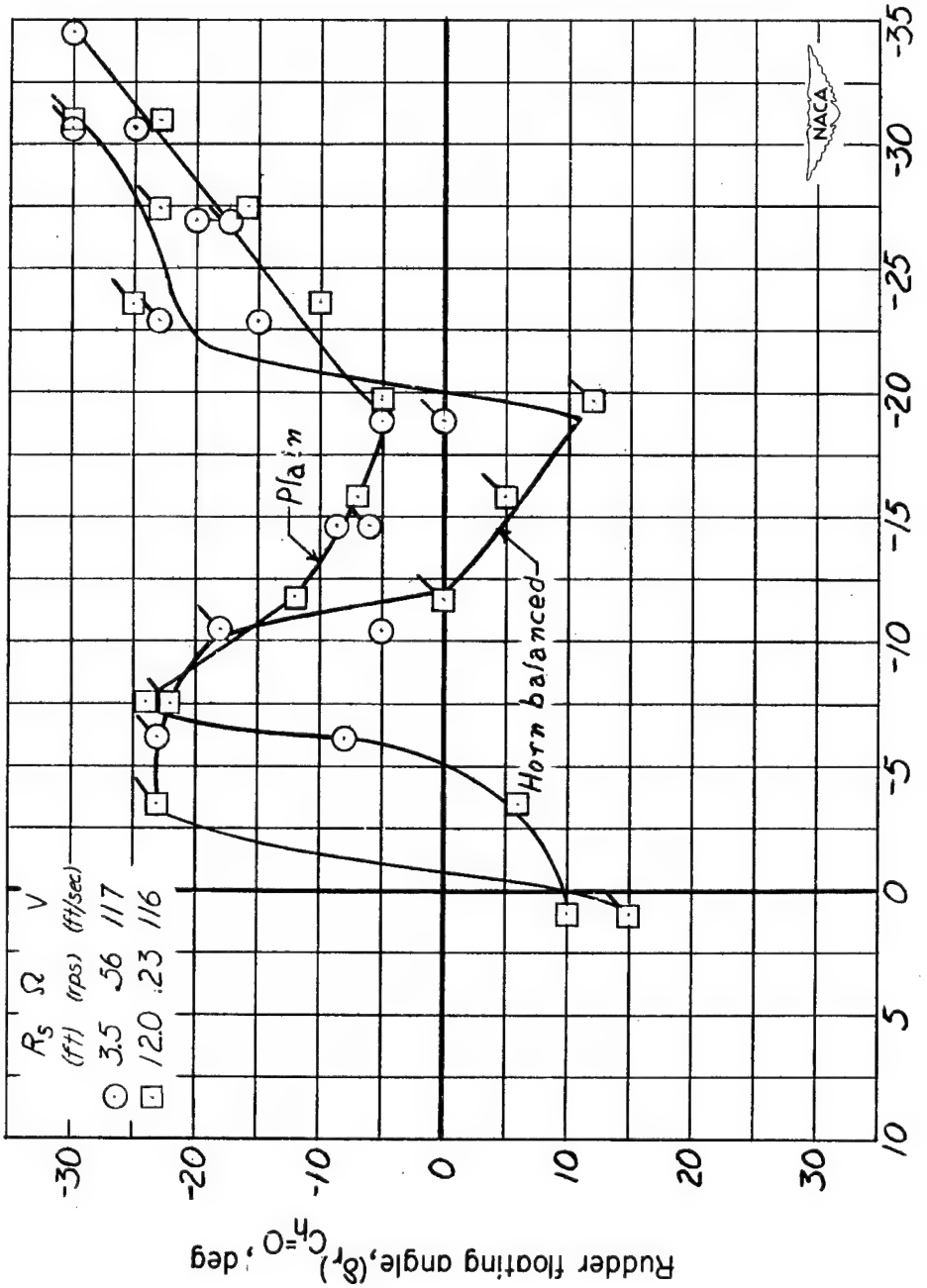

(e) $\alpha = 55^\circ$.

Figure 7.- Continued.

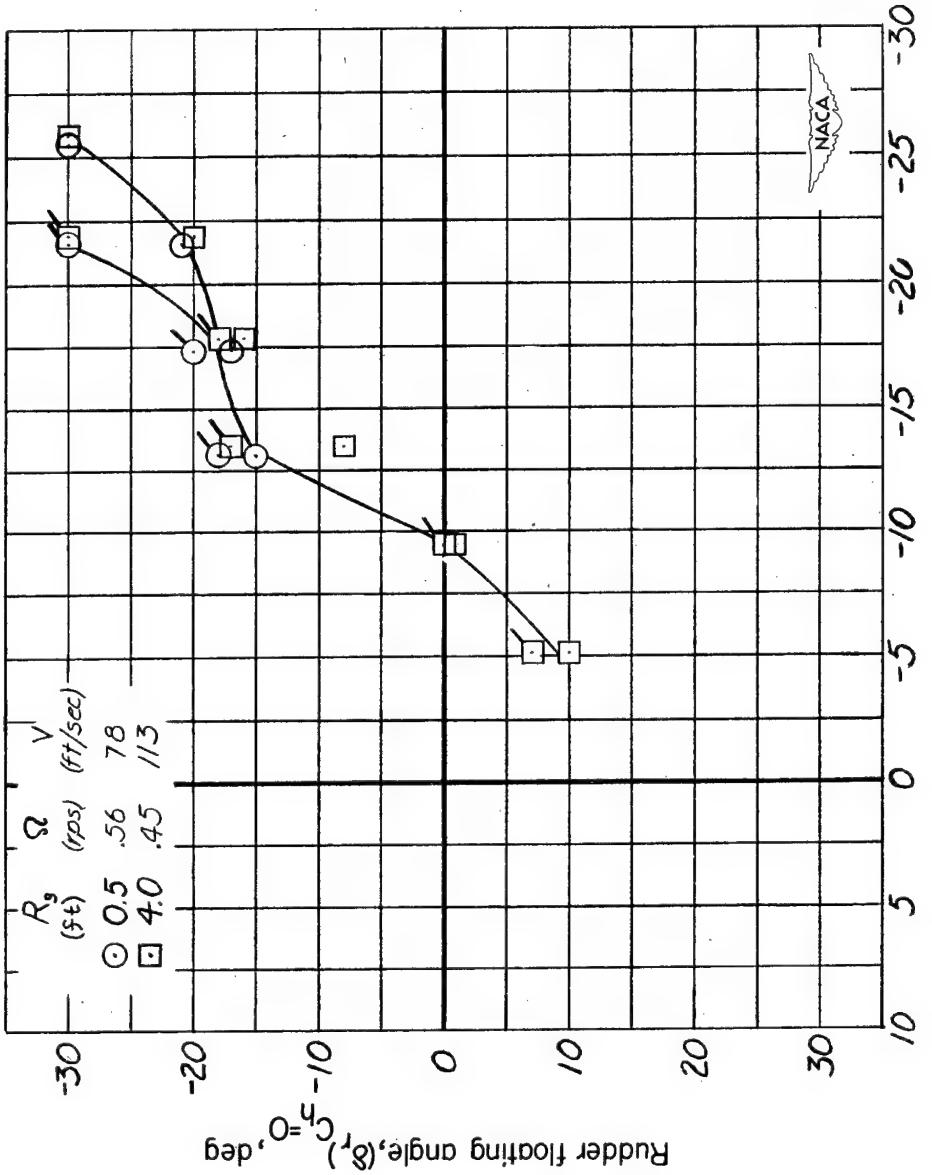

(f) $\alpha = 65^\circ$.

Figure 7.- Concluded.

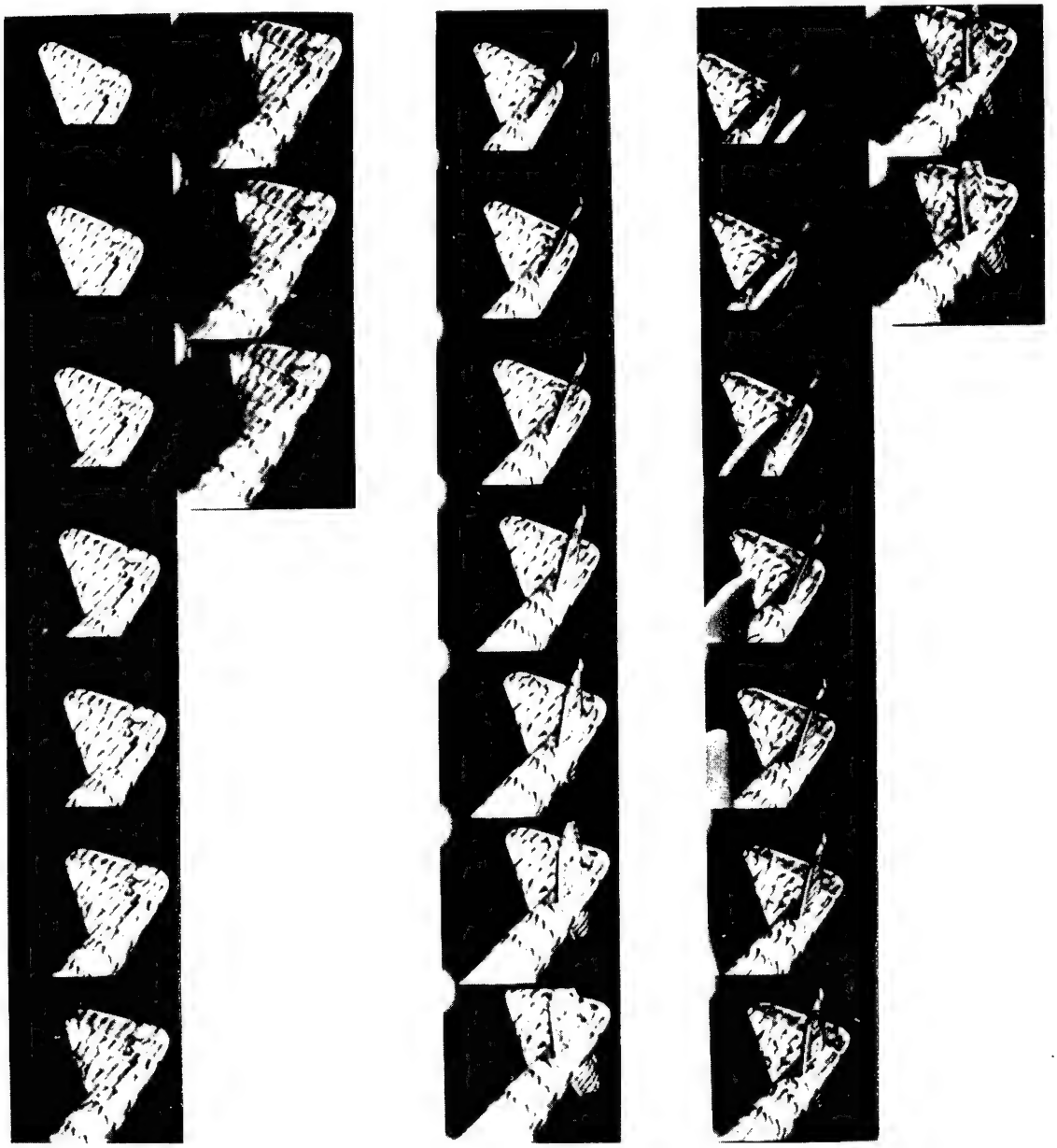

Wing and horizontal tail removed | Wing removed | Complete model

NACA L-69096

(a) $\beta_t = 1.7^\circ$ (test 67).

Figure 8.- Motion pictures of tufts on outboard side of tail for all model configurations. Horn-balanced rudder; angle of attack, 35°.

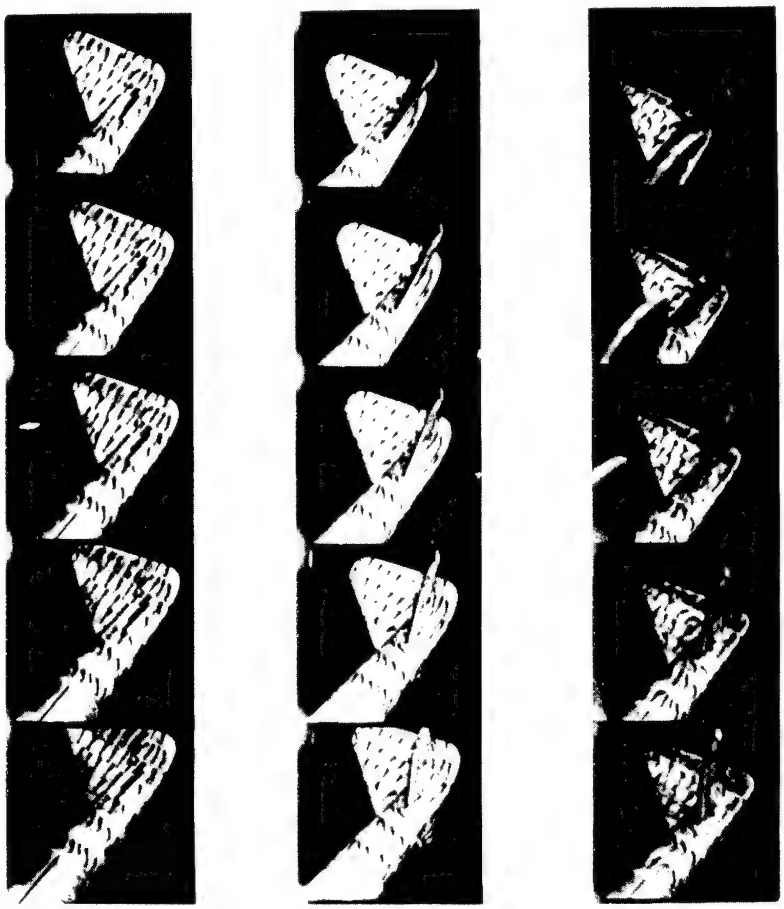

Wing and horizontal tail removed | Wing removed | Complete model

(b) $\beta_t = -3.3^\circ$ (test 58).

Figure 8.- Continued.

NACA L-69097

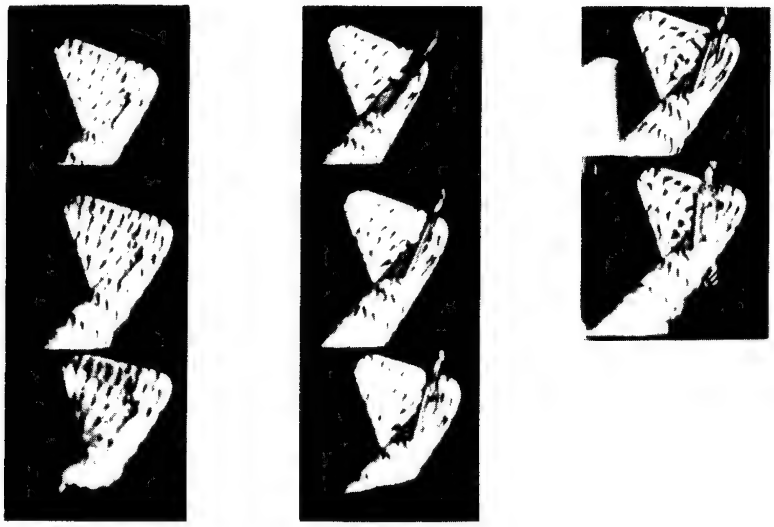

Wing and horizontal tail removed | Wing removed | Complete model

(c) $\beta_t = -10.3^\circ$ (test 49).

Figure 8.- Continued.

NACA L-69098

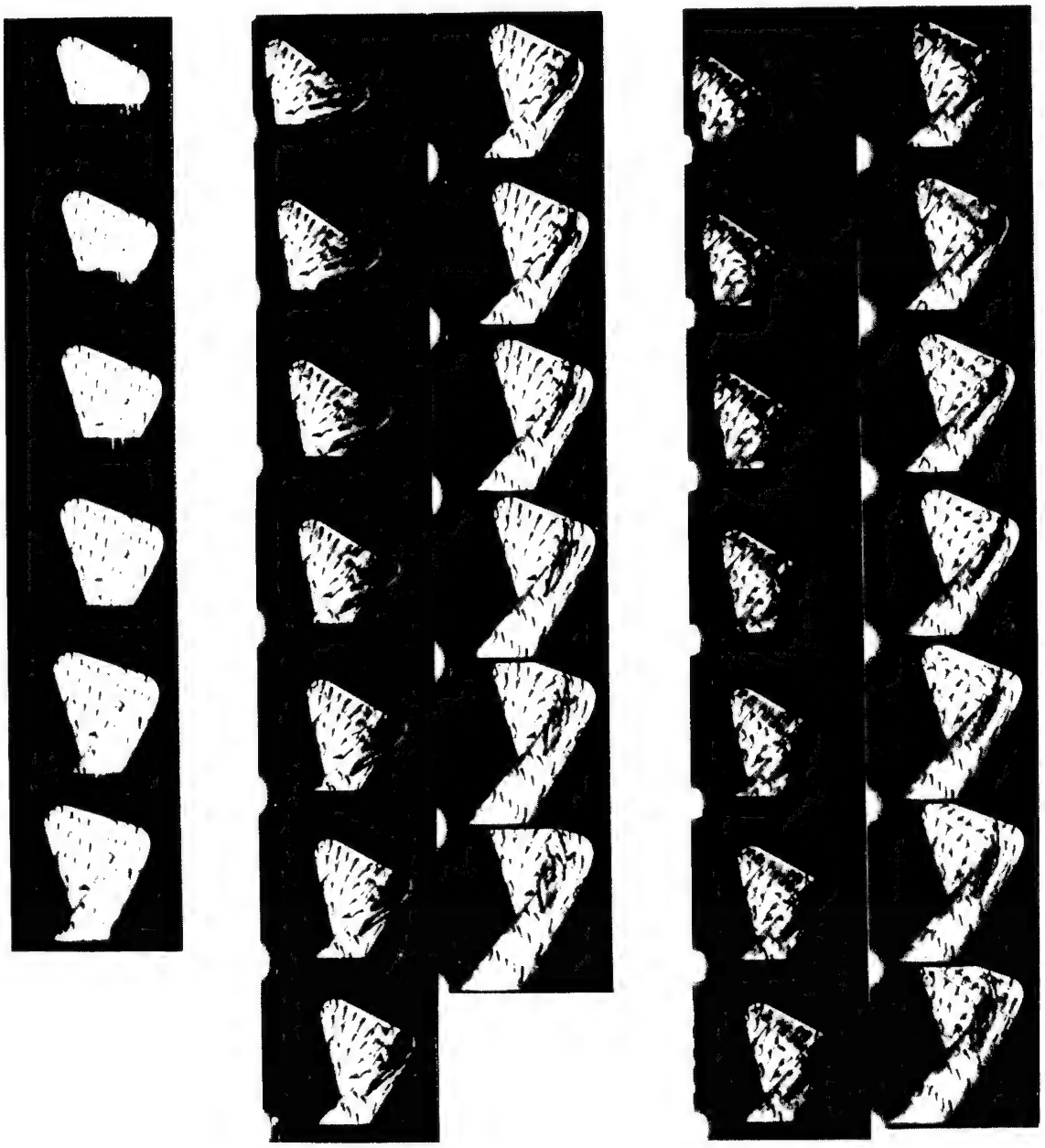

Wing and horizontal tail removed | Wing removed | Complete model

(d) $\beta_t = -18.5^\circ$ (test 62).

Figure 8.- Continued.

NACA L-69099

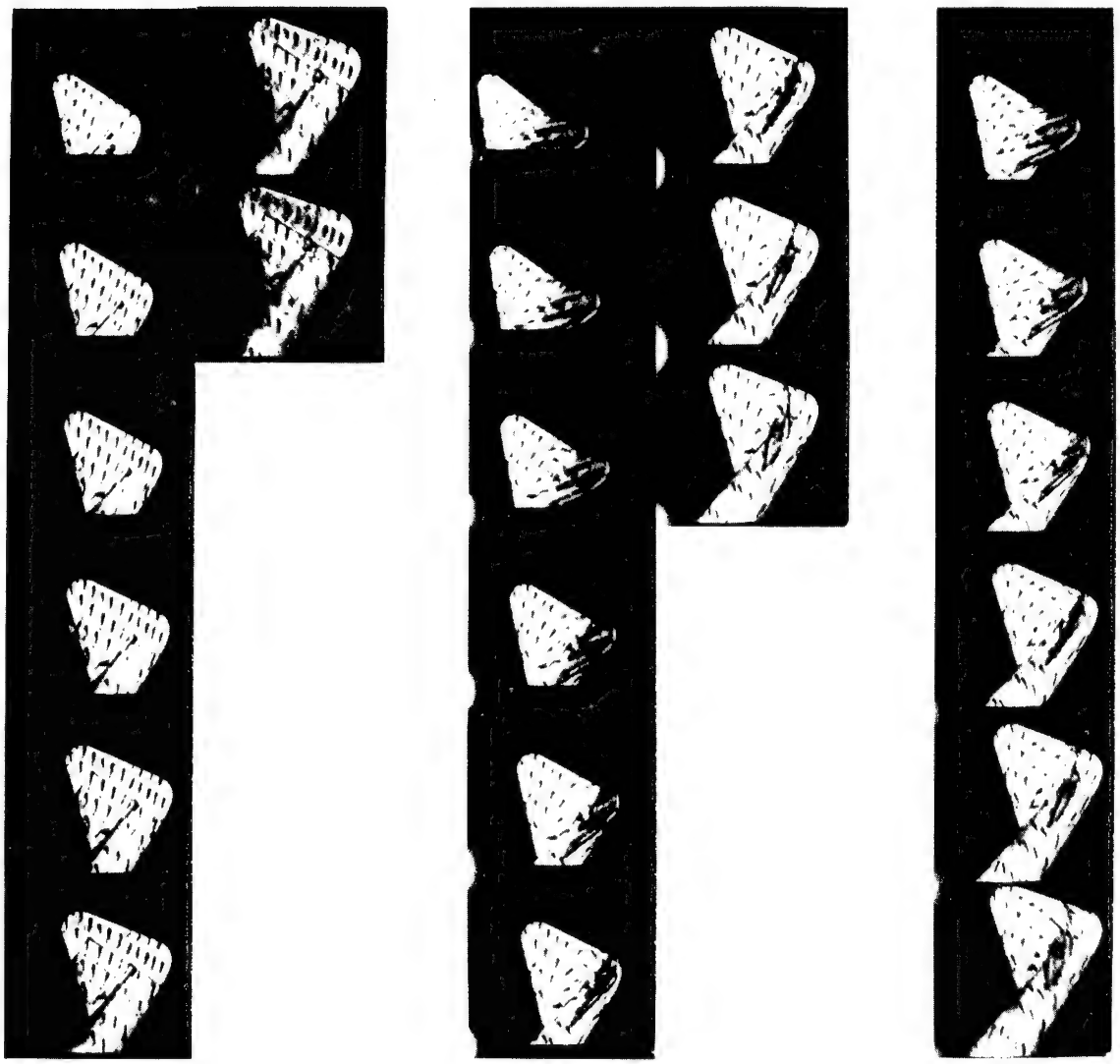

Wing and horizontal tail removed | Wing removed | Complete model

(e) $\beta_t = -23.5^\circ$ (test 53).

NACA L-69100

Figure 8.- Continued.

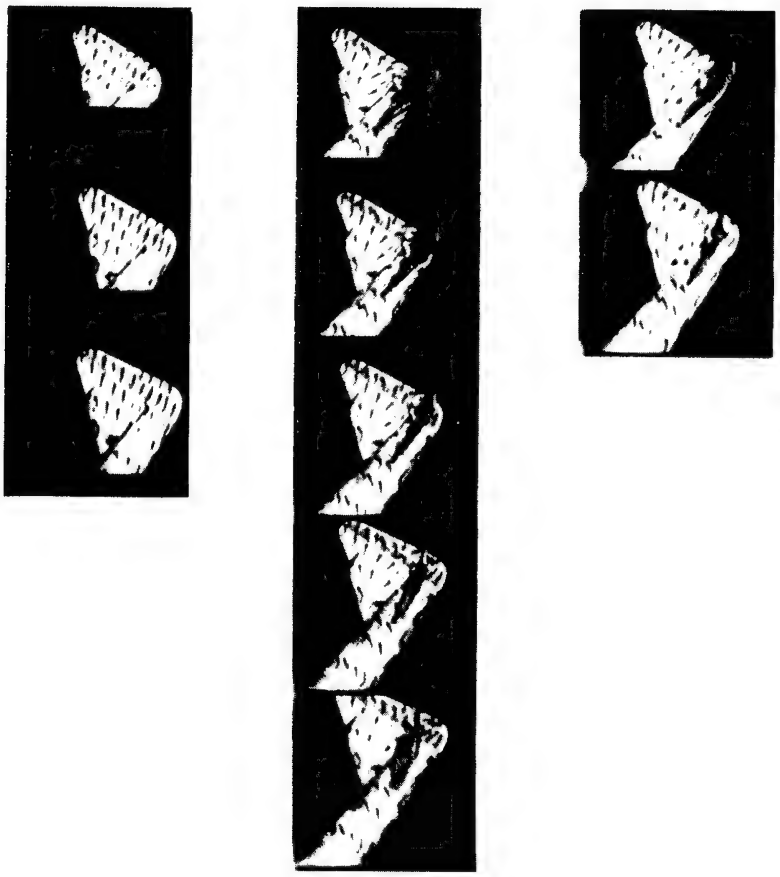

Wing and horizontal tail removed | Wing removed | Complete model

(f) $\beta_t = -30.6^\circ$ (test 44).

Figure 8.- Concluded.

NACA L-69101

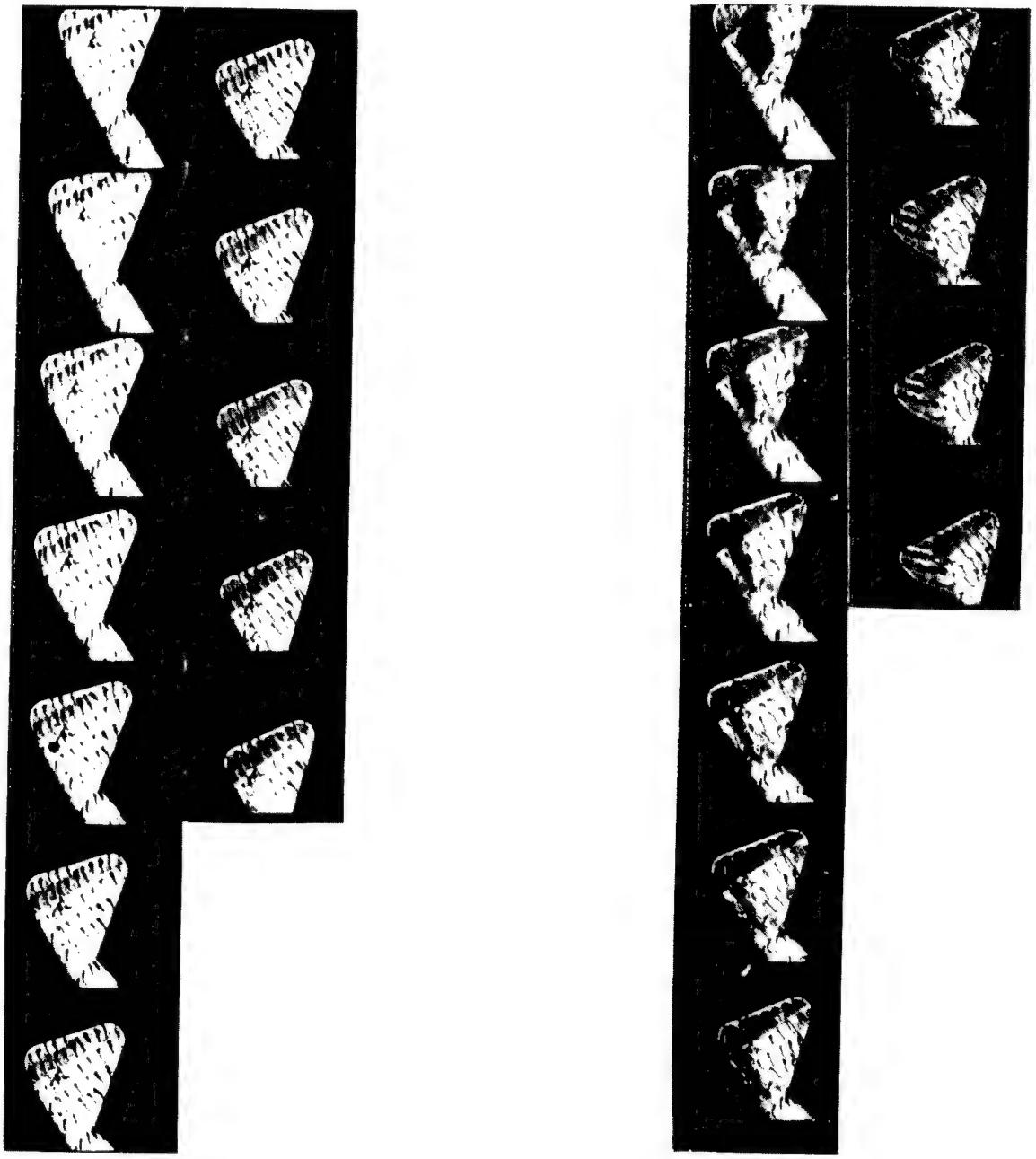

Wing and horizontal tail removed

Complete model

NACA

L-69102

(a) $\beta_t = 1.7^\circ$ (test 67).

Figure 9.- Motion pictures of tufts on inboard side of tail for all model configurations. Horn-balanced rudder; angle of attack, 35°.

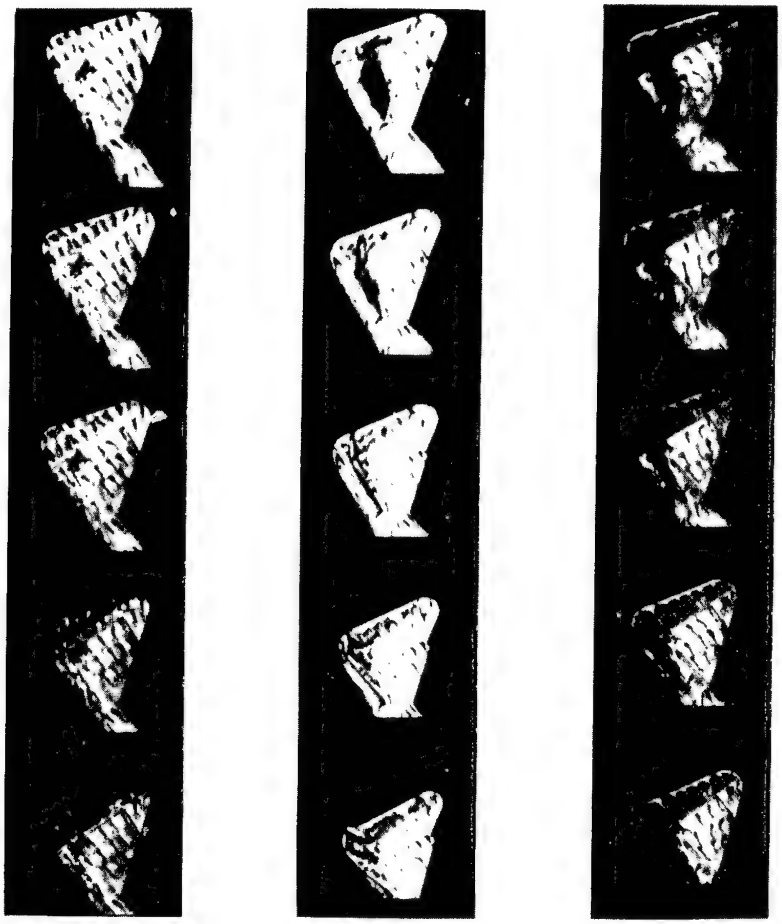

Wing and horizontal tail removed | Wing removed | Complete model

(b) $\beta_t = -3.3^\circ$ (test 58).

Figure 9.- Continued.

NACA L-69103

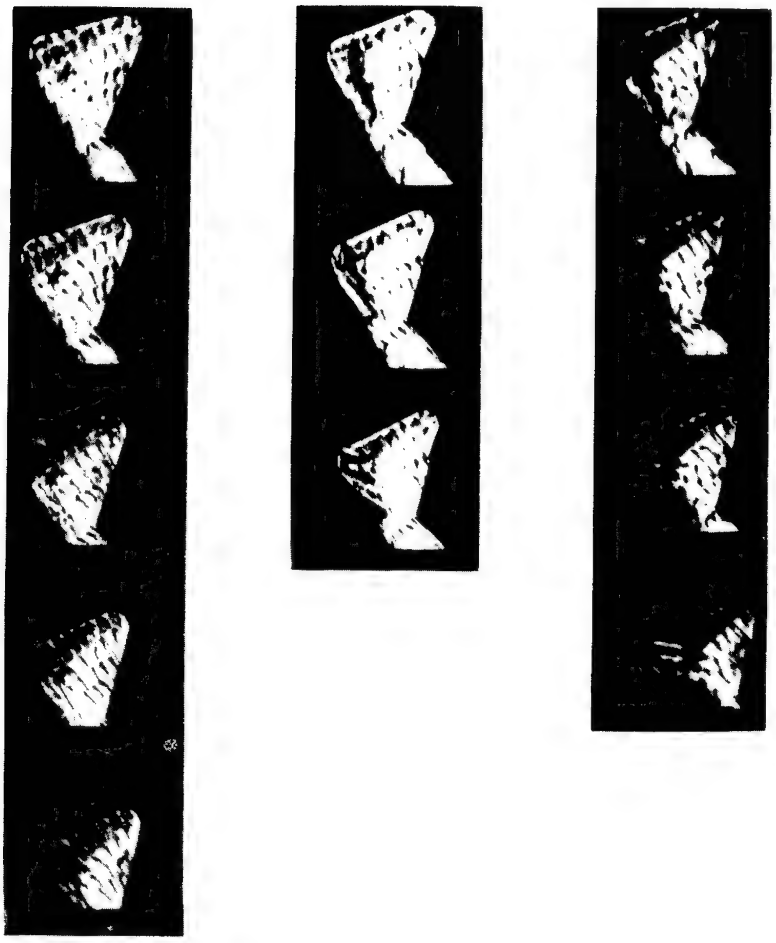

Wing and horizontal tail removed | Wing removed | Complete model

(c) $\beta_t = -10.3^\circ$ (test 49).

Figure 9.- Continued.

NACA L-69104

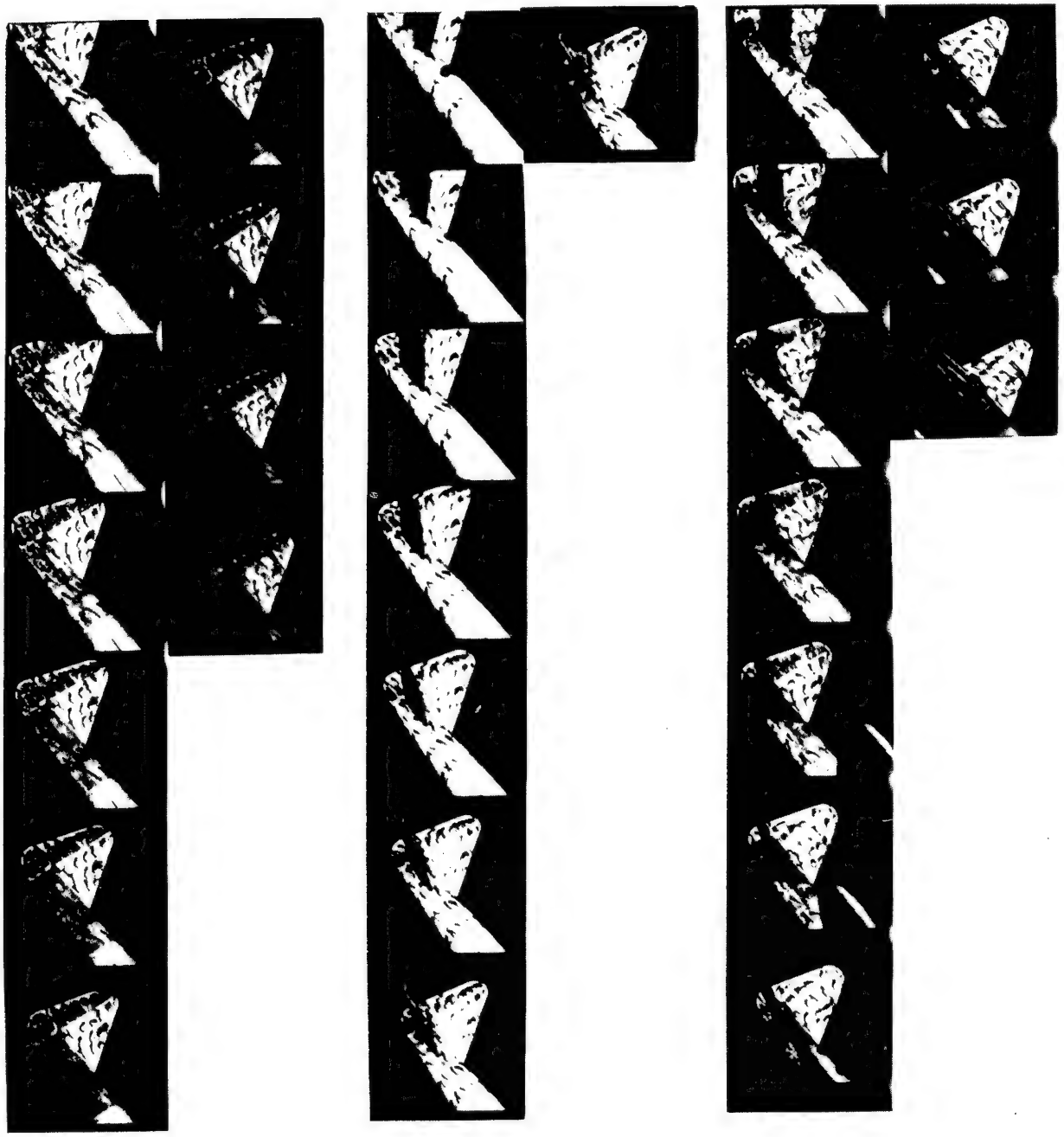

Wing and horizontal tail removed | Wing removed | Complete model

(d) $\beta_t = -18.5^\circ$ (test 62).

Figure 9.- Continued.

L-69105

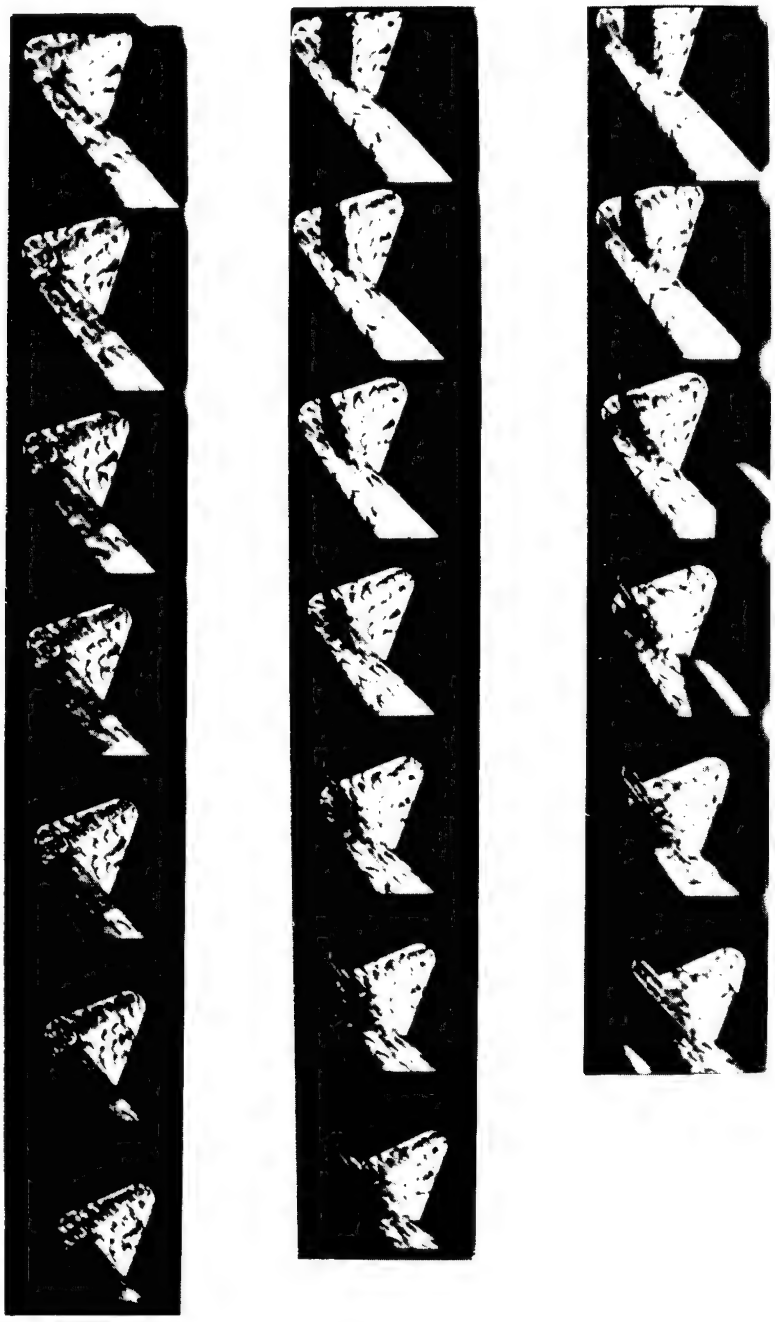

Wing and horizontal tail removed | Wing removed | Complete model

(e) $\beta_t = -23.5^\circ$ (test 53).

Figure 9.- Continued.

L-69106

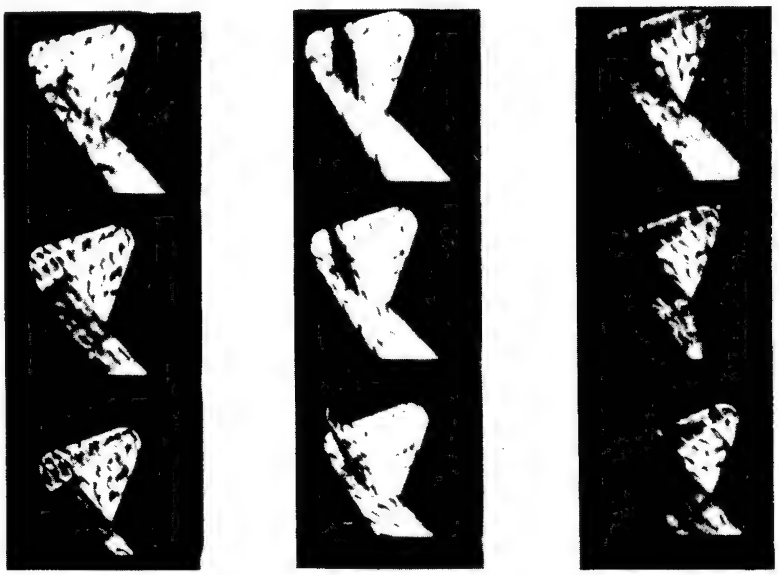

Wing and horizontal tail removed | Wing removed | Complete model

(f) $\beta_t = -30.6^\circ$ (test 44).

Figure 9.- Concluded.

L-69107

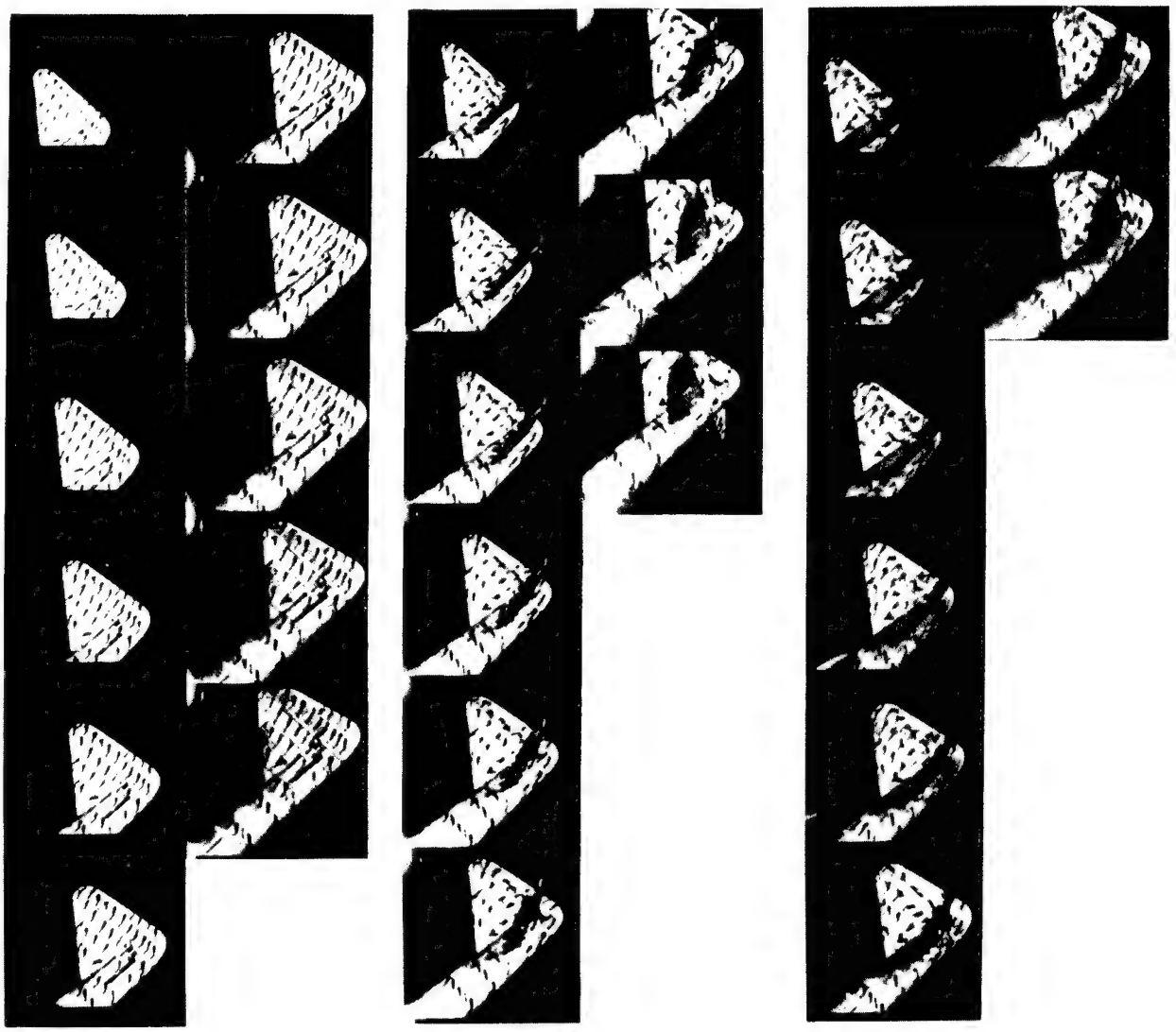

Wing and horizontal tail removed | Wing removed | Complete model

(a) $\beta_t = -7.7^\circ$ (test 92).

L-69108

Figure 10.- Motion pictures of tufts on outboard side of tail for all model configurations. Horn-balanced rudder; angle of attack, 45°.

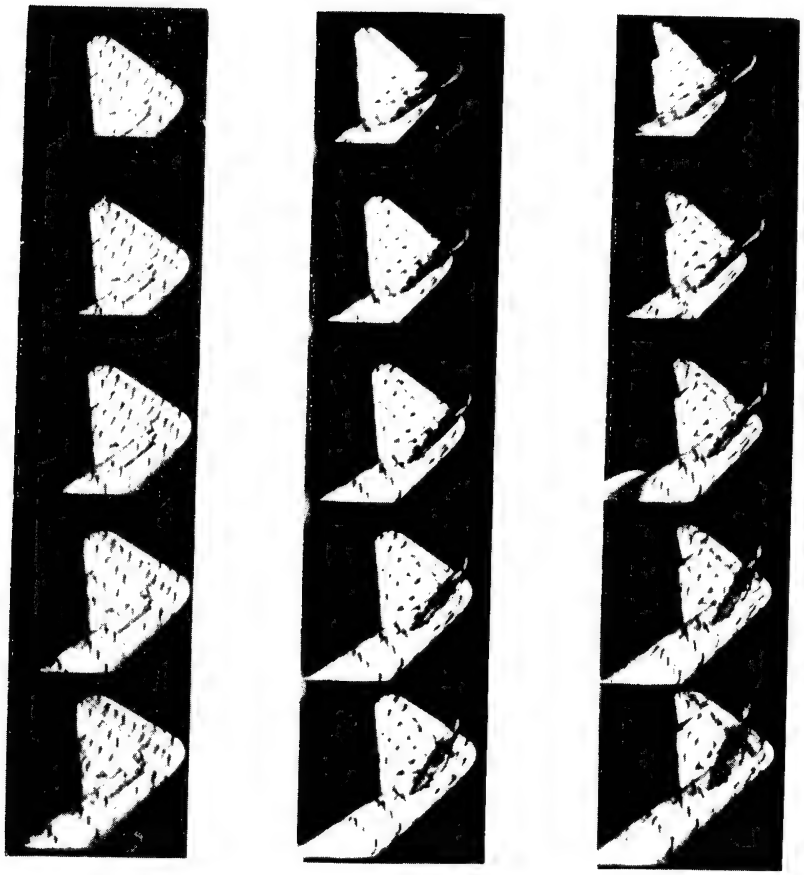

Wing and horizontal tail removed | Wing removed | Complete model

(b) $\beta_t = -13.3^\circ$ (test 83).

Figure 10.- Continued.

NACA L-69709

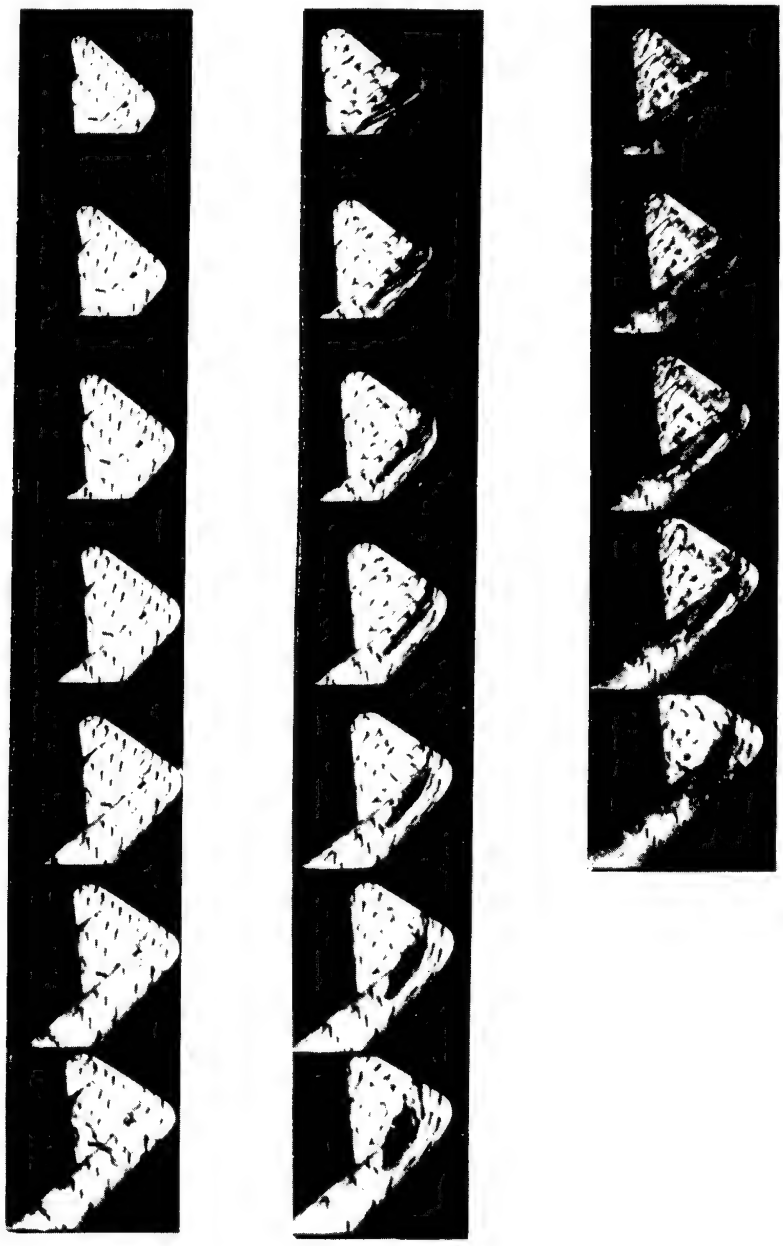

Wing and horizontal tail removed | Wing removed | Complete model

(c) $\beta_t = -21.3^\circ$ (test 81).

Figure 10.- Continued.

NACA L-69110

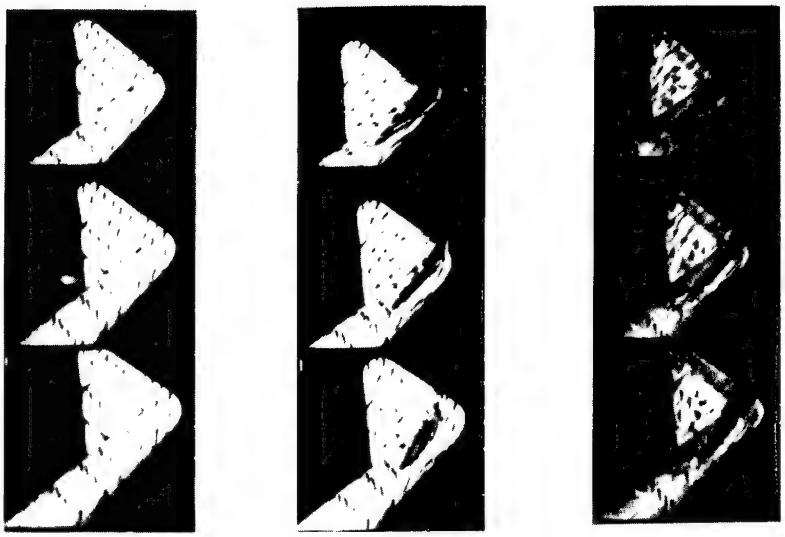

Wing and horizontal tail removed | Wing removed | Complete model

(d) $\beta_t = -29.0^\circ$ (test 72).

Figure 10.- Concluded.

L-69111

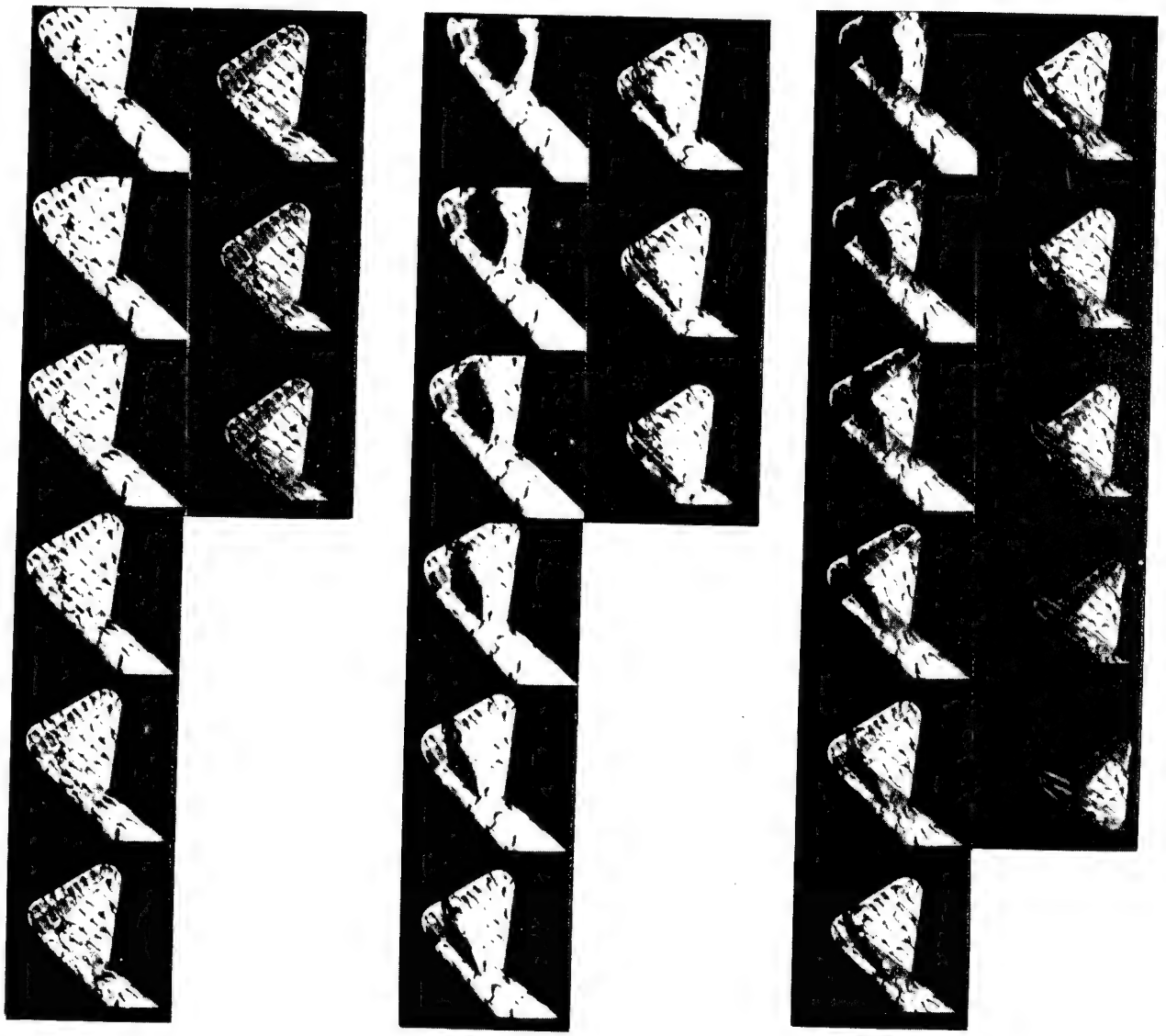

Wing and horizontal tail removed | Wing removed | Complete model

(a) $\beta_t = -7.7^\circ$ (test 92).

NACA L-69112

Figure 11.- Motion pictures of tufts on inboard side of tail for all model configurations. Horn-balanced rudder; angle of attack, 45°.

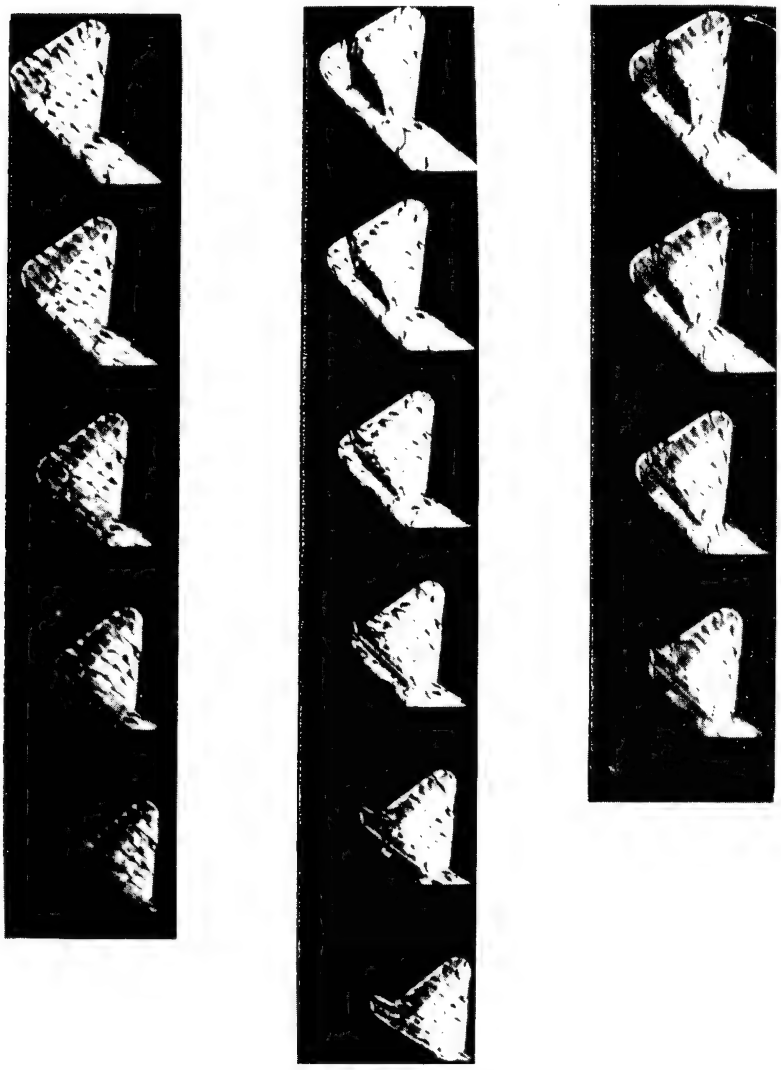

Wing and horizontal tail removed | Wing removed | Complete model

(b) $\beta_t = -13.3^\circ$ (test 83).

NACA L-69113

Figure 11.- Continued.

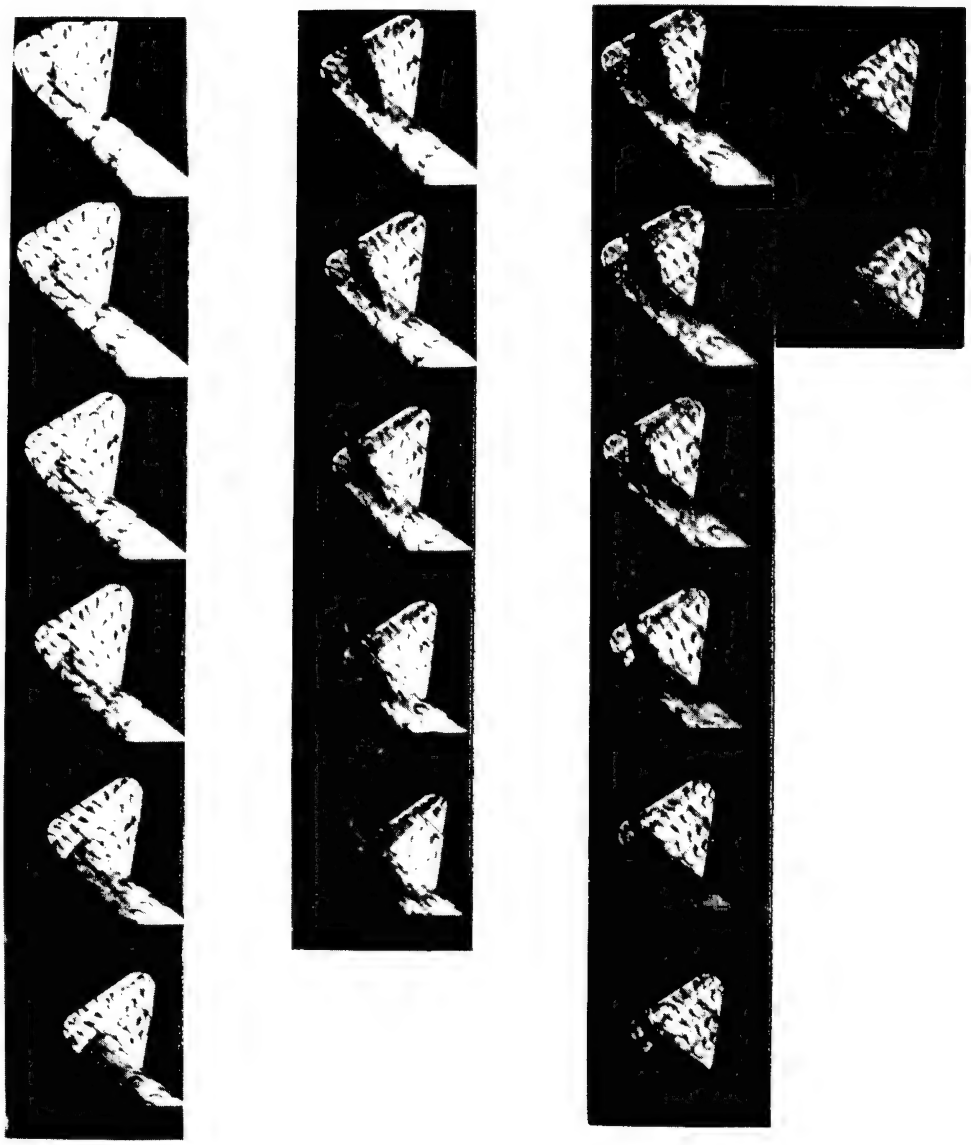

Wing and horizontal tail removed | Wing removed | Complete model

(c) $\beta_t = -21.3^\circ$ (test 81).

Figure 11.- Continued.

L-69114

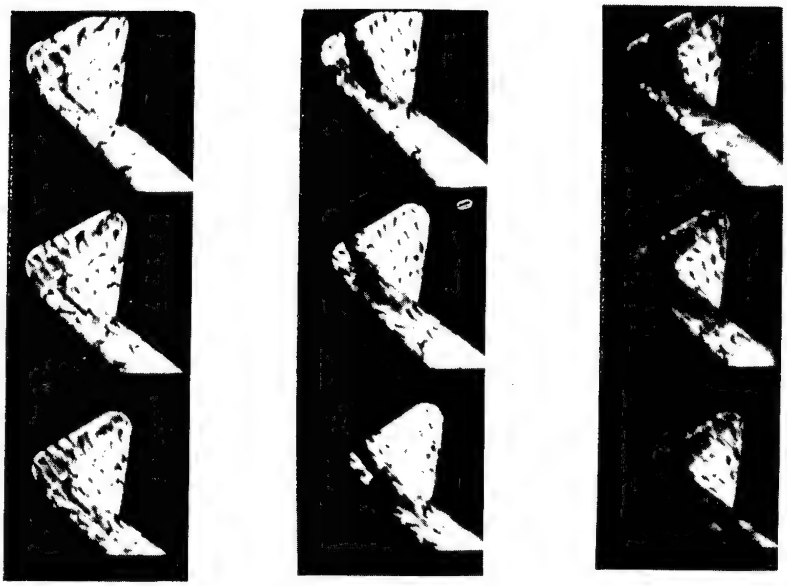

Wing and horizontal tail removed | Wing removed | Complete model

(d) $\beta_t = -29.0^\circ$ (test 72).

Figure 11.- Concluded.

L-69115

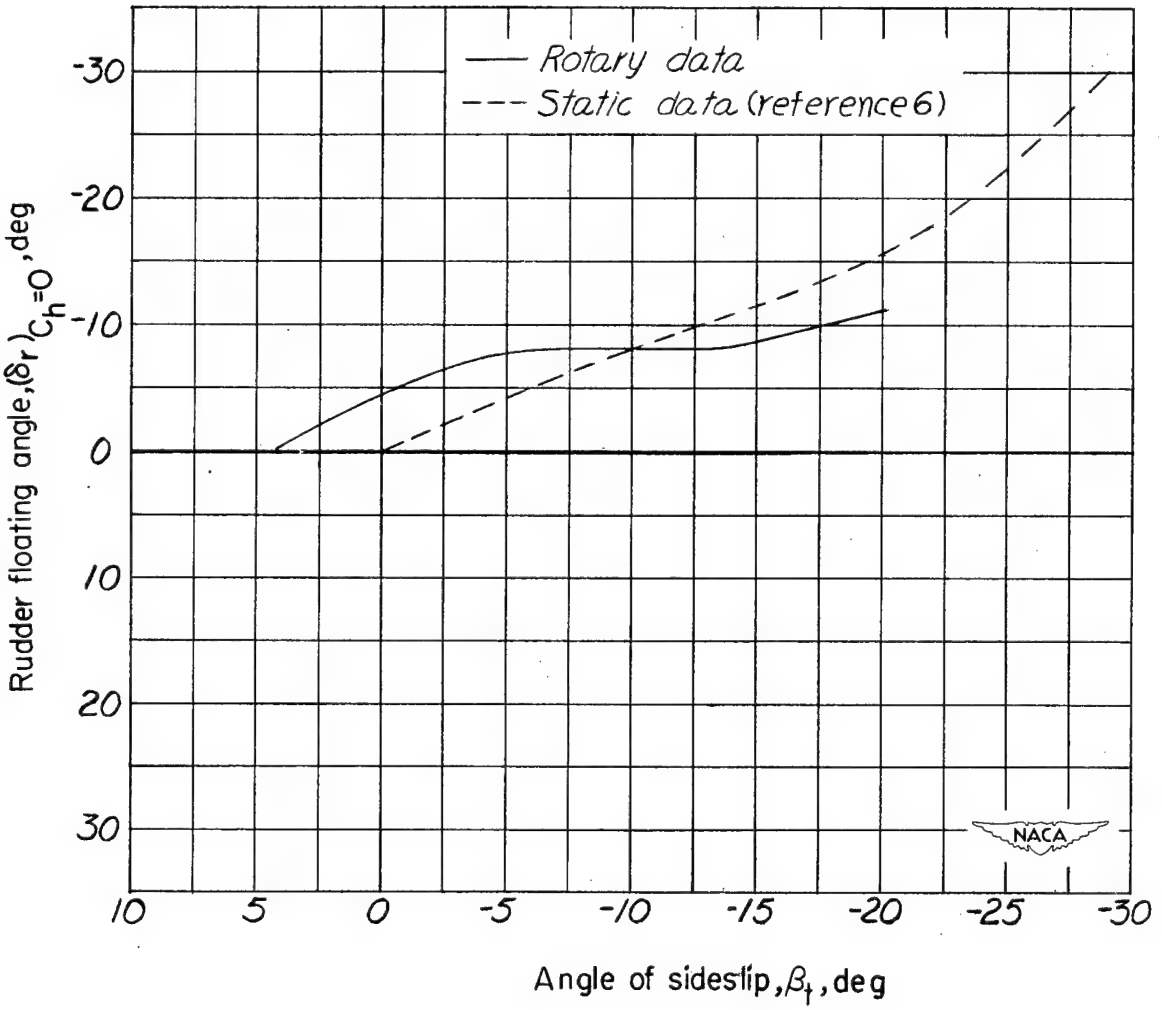

(a) $\alpha = 15^\circ$.

Figure 12.- Comparison of plain-rudder static and rotary data obtained without a horizontal tail and wing. Rudder floating angles plotted as a function of sideslip at the tail for specific angles of attack.

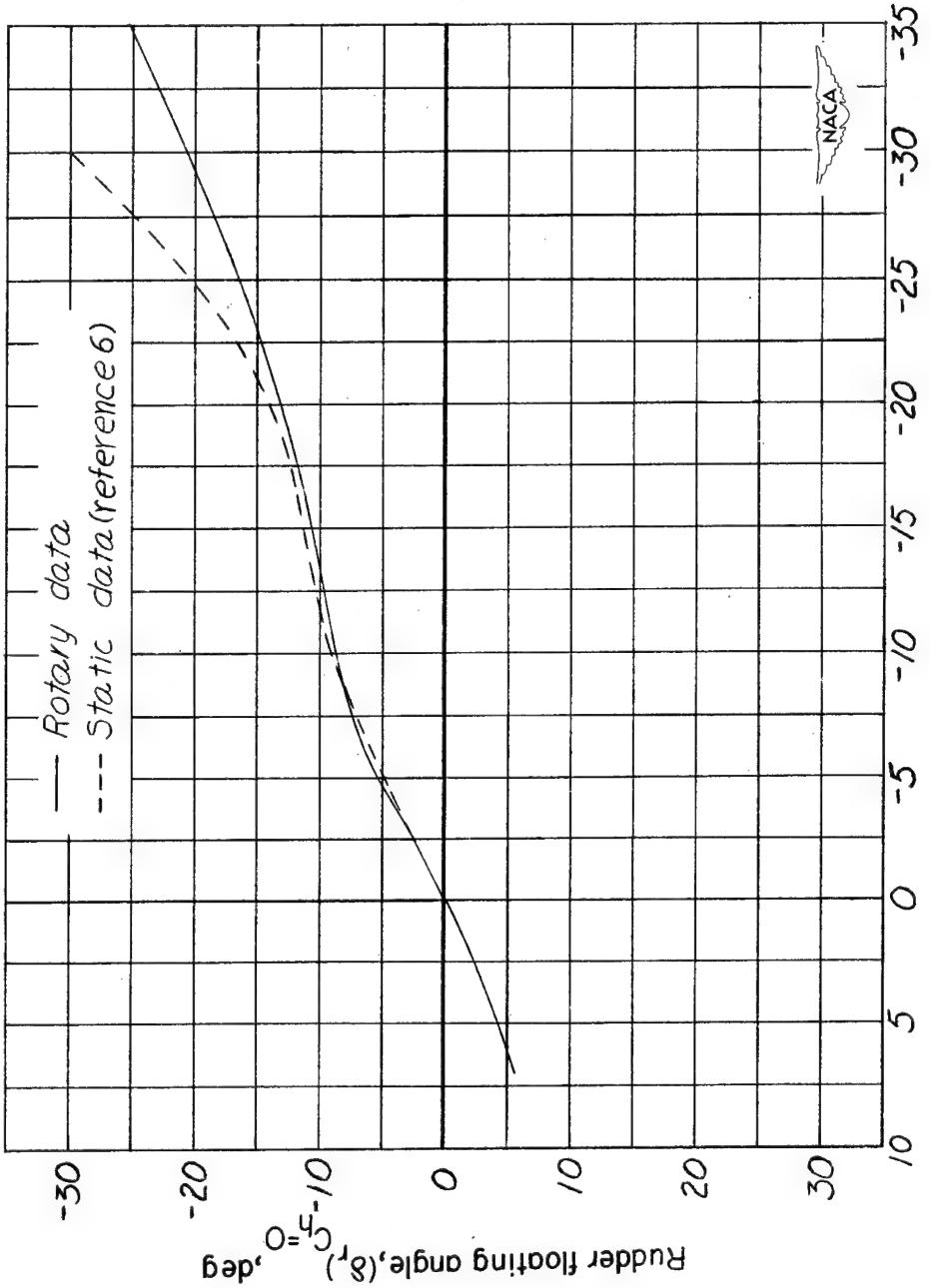

(b) $\alpha = 25°$.

Figure 12.- Continued.

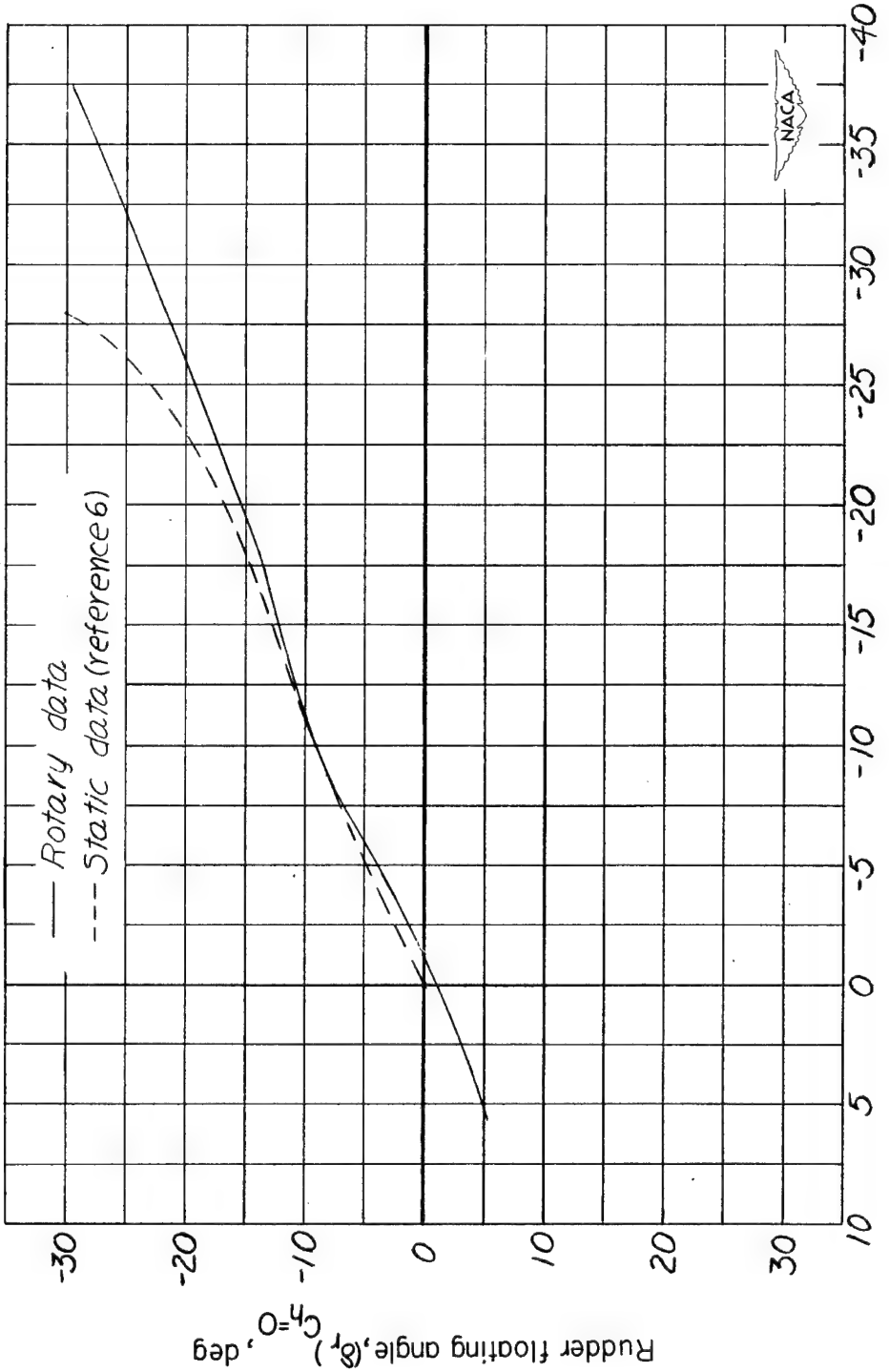

(c) $\alpha = 35°$.

Figure 12.- Continued.

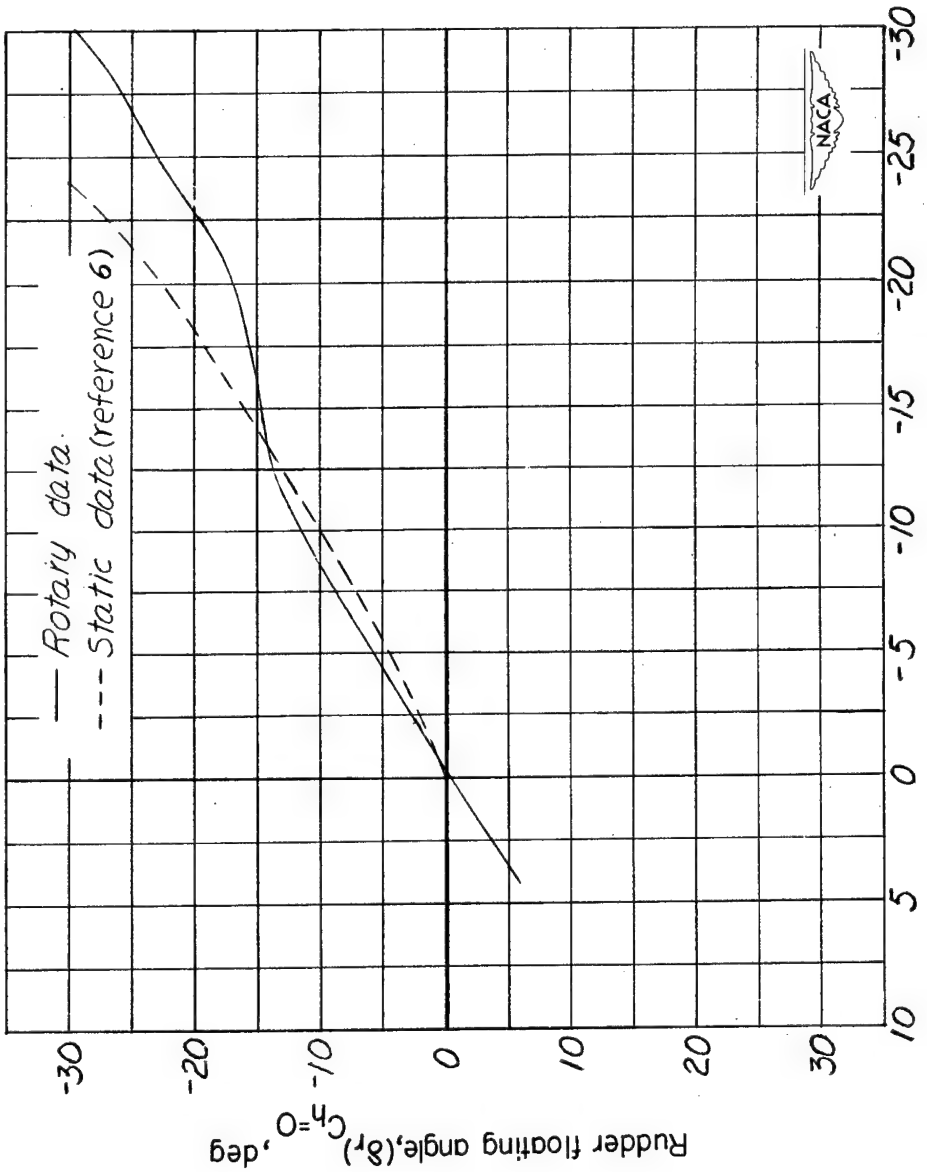

(d) $\alpha = 45^\circ$.

Figure 12.- Continued.

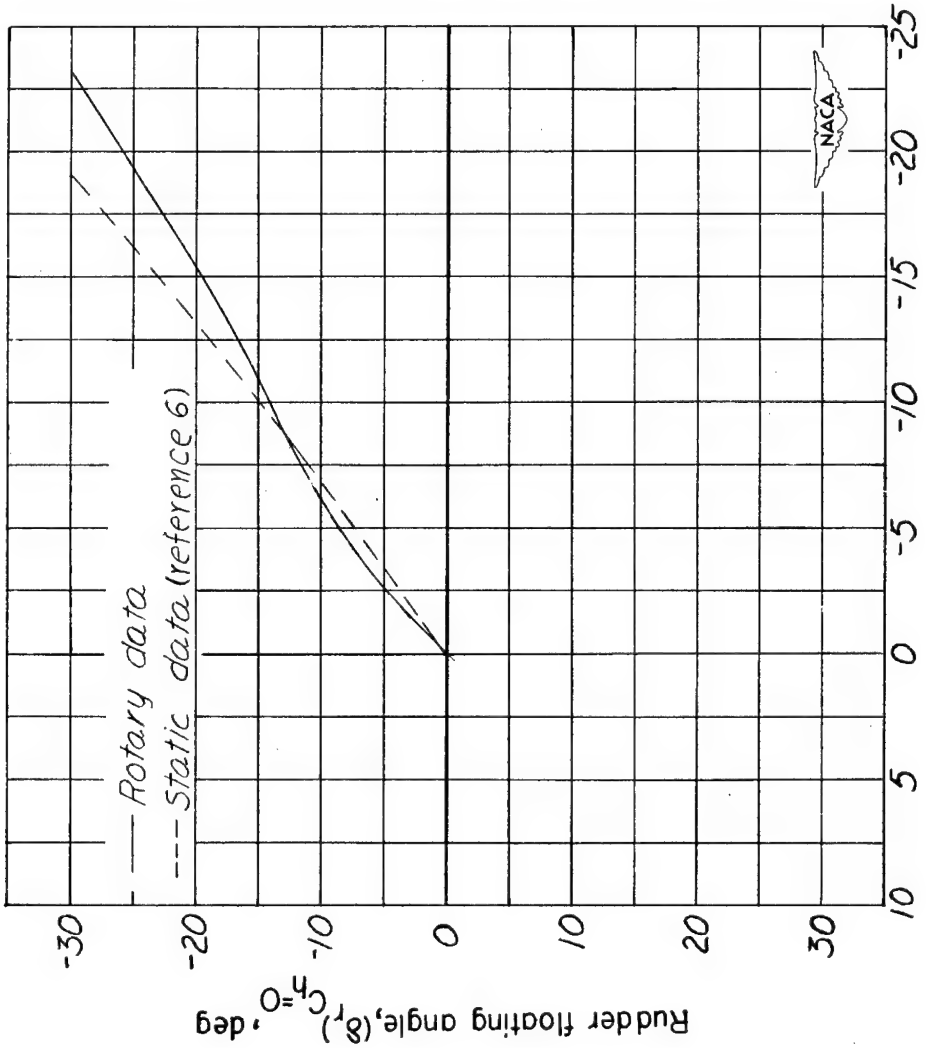

(e) $\alpha = 55°$.

Figure 12.- Continued.

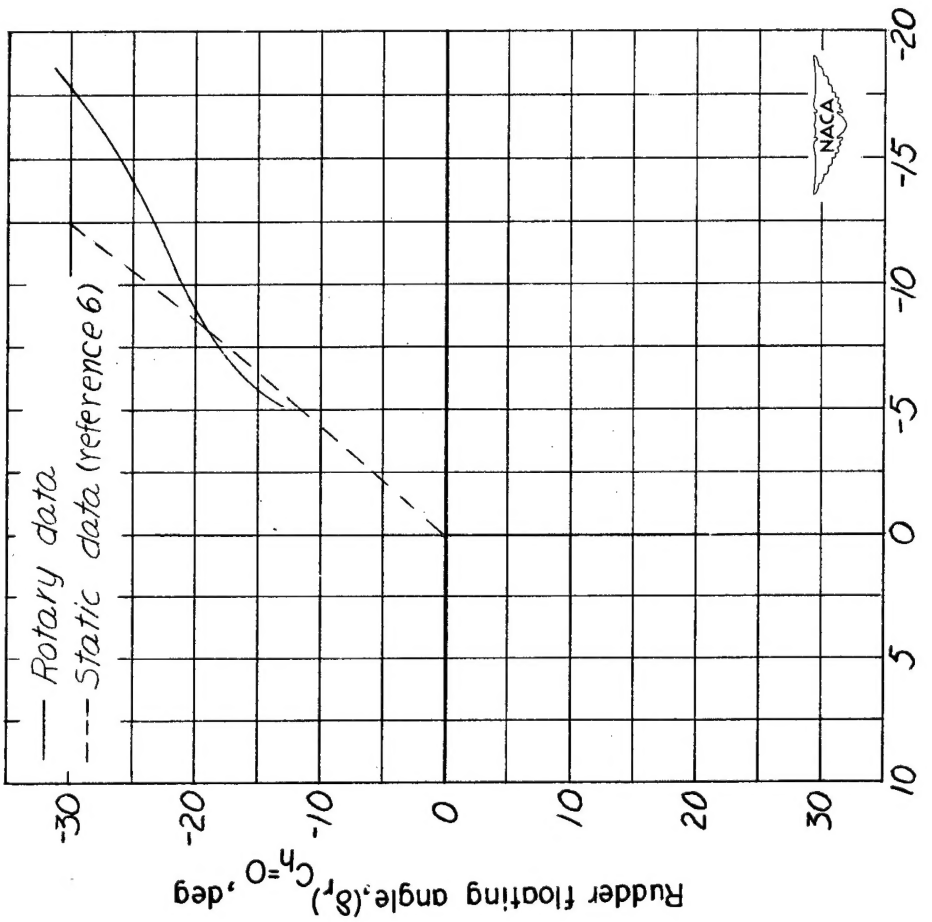

(f) $\alpha = 65°$.

Figure 12.- Concluded.

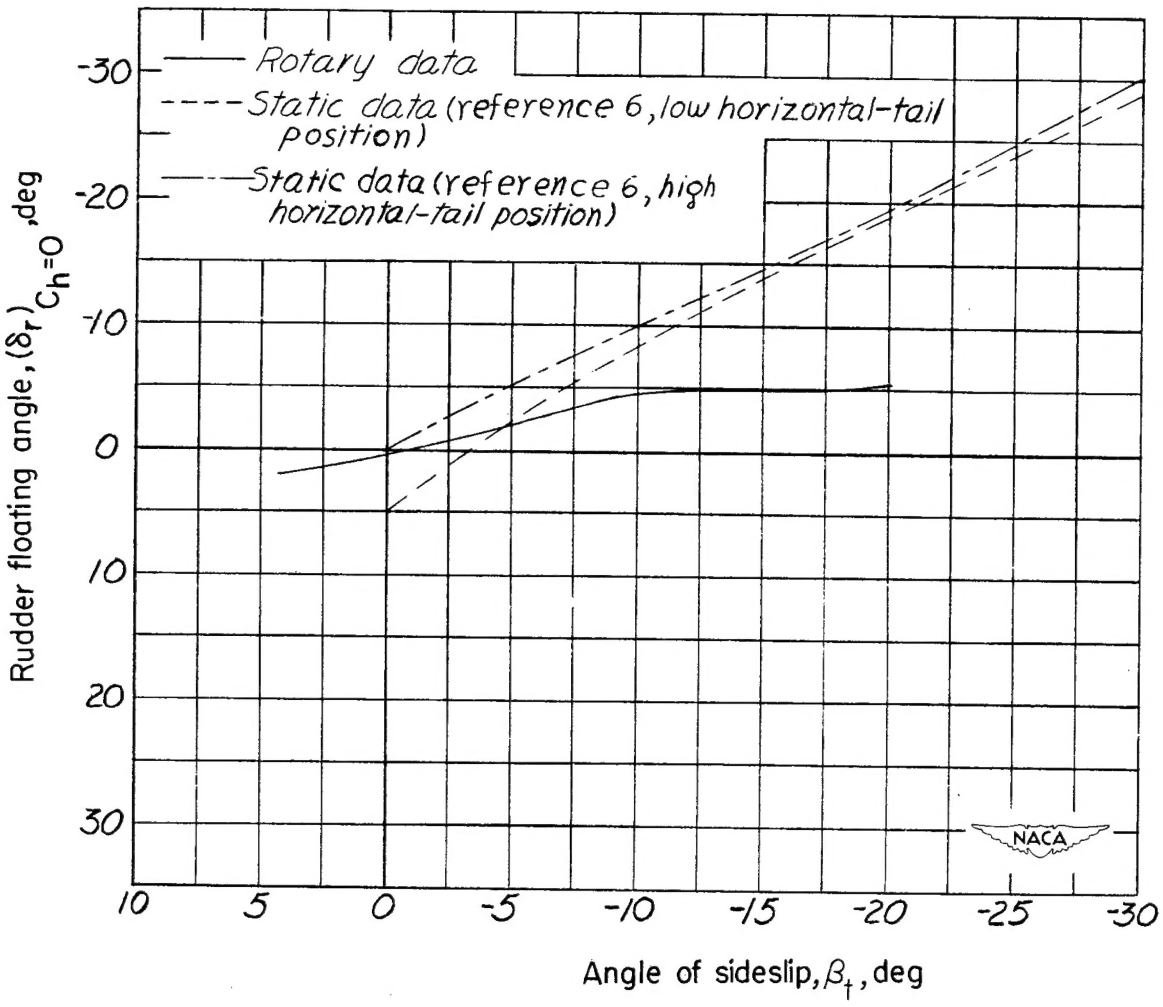

(a) $\alpha = 15^\circ$.

Figure 13.- Comparison of plain-rudder static and rotary data obtained without a wing. Rudder floating angles plotted as a function of sideslip at the tail for specific angles of attack.

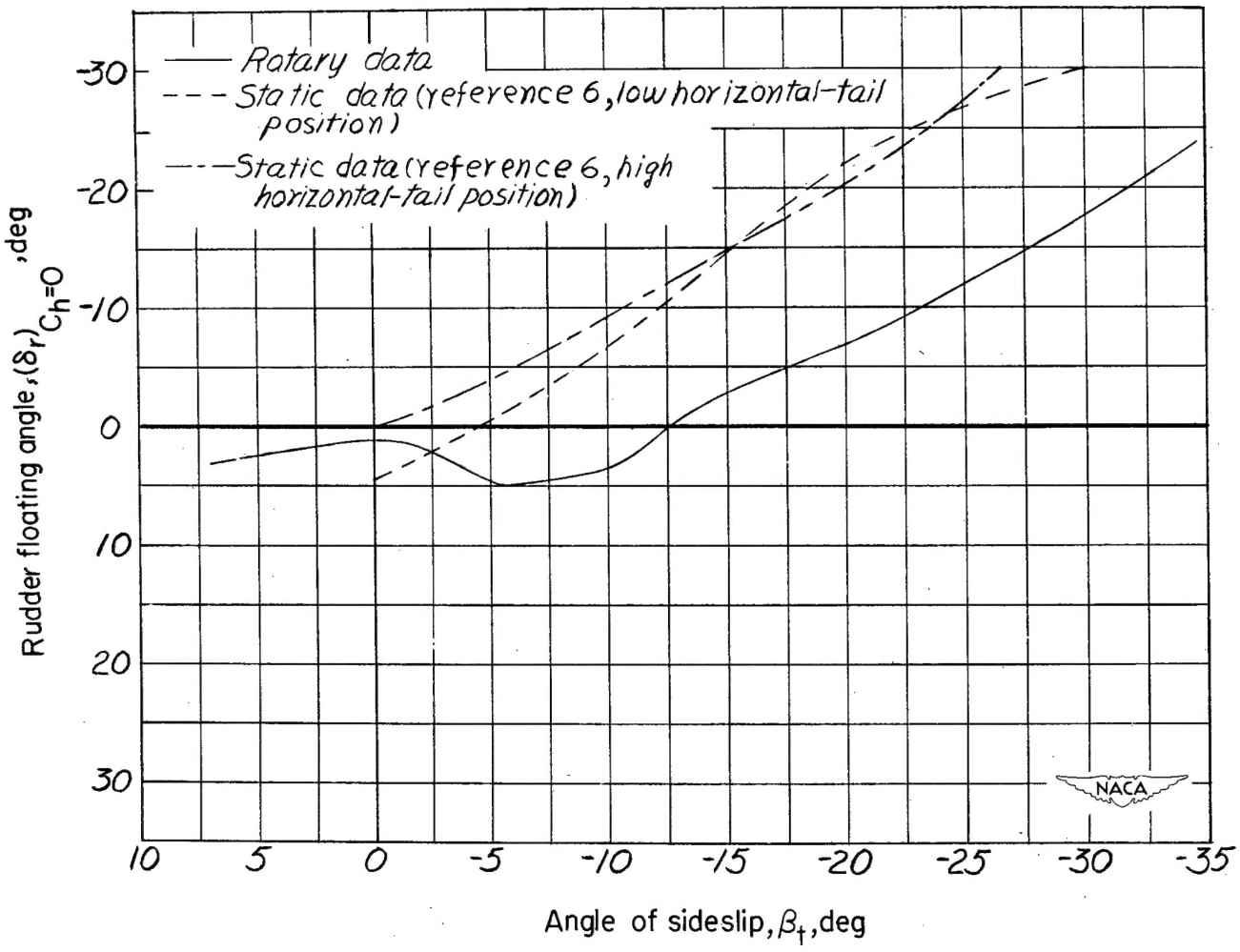

(b) $\alpha = 25^\circ$.

Figure 13.- Continued.

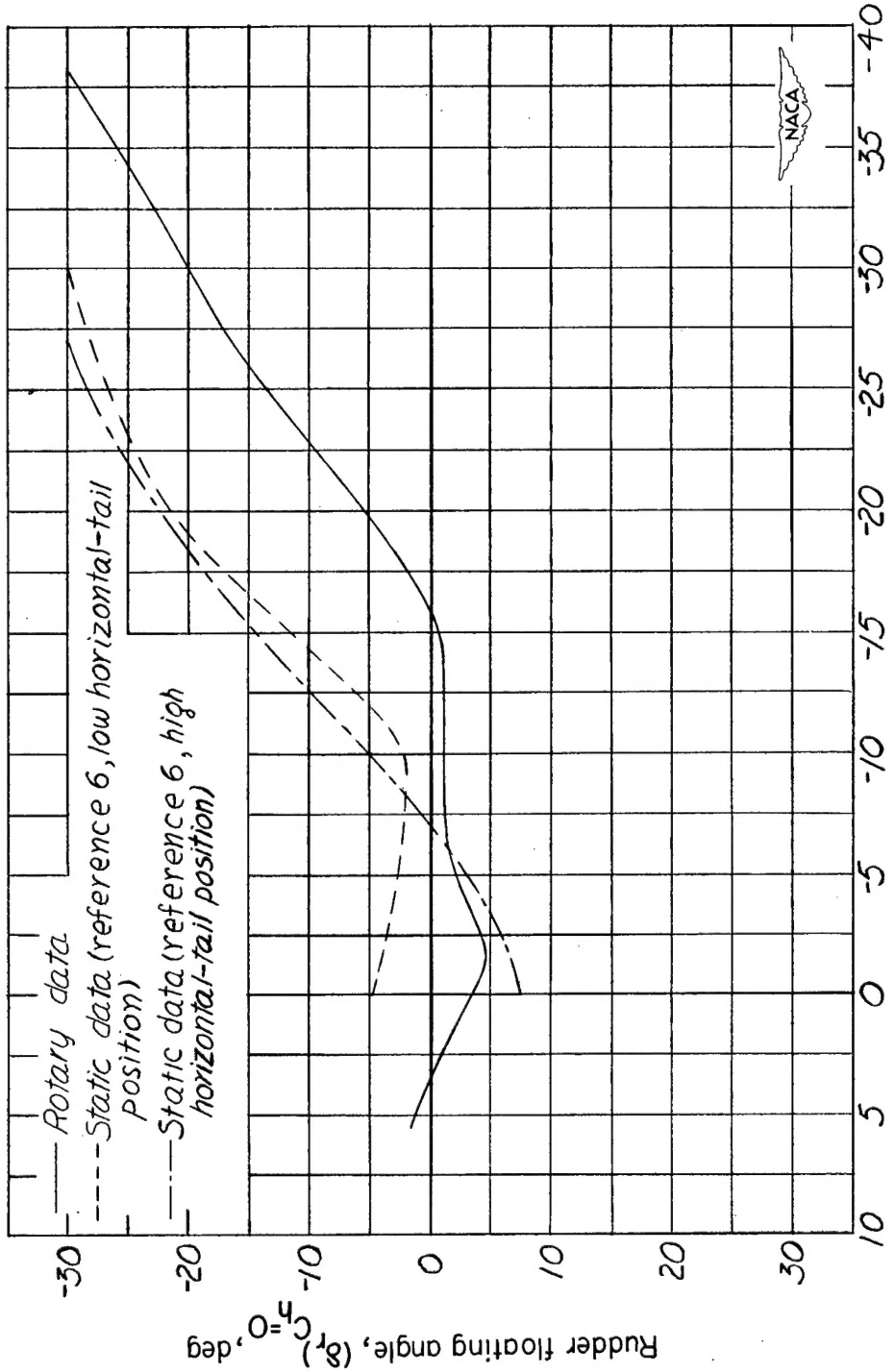

(c) $\alpha = 35^\circ$.

Figure 13.- Concluded.